Comparing Secondary Organic Aerosols Schemes Implemented in Current Chemical Transport Models and the Policy Implications of Uncertainties

Ling Huang[1], Benjie Chen[1], Zi'ang Wu[1], Katie Tuite[2], Pradeepa Vennam[2], Greg Yarwood[2,*], Li Li[1,*]

[1]School of Environmental and Chemical Engineering, Shanghai University, Shanghai, 200444, China

[2]Ramboll, Novato, California, 94945, USA

Correspondence to: Greg Yarwood (gyarwood@ramboll.com), Li Li (lily@shu.edu.cn)

Abstract

Secondary organic aerosol (SOA) constitutes a major component of fine particulate matter ($PM_{2.5}$) that models must account for to assess how human activities influence air quality, climate, and public health. We characterize the current state of SOA modeling by analyzing eight SOA schemes implemented in five widely used air quality models: CAMx, CMAQ, GEOS-Chem, WRF-Chem and CHIMERE. We performed offline calculations to compare ~~initial~~non-aged SOA yields, the effects of SOA aging processes, and the influence of NOx conditions on yields. Our objective is to understand variation rather than to identify a superior scheme. We find significant discrepancies in ~~initial~~ SOA yields ~~leading to different precursor rankings of SOA-forming potential.~~ ~~T~~with the ratio of maximum to minimum ~~initial~~non-aged yield spannings~~~~ from 1.8 to over 1000, depending upon precursor~~, with the median of 4.2 underscoring large uncertainties~~. The impact of nitrogen oxide (NOx) conditions on SOA yields is also highly variable among schemes. While some schemes include SOA aging, their treatments differ substantially, with some schemes showing large increases in SOA mass, while others exhibit minimal changes. Box model simulations confirmed the substantial discrepancies in predicted SOA concentrations and their responses to precursor emission changes. The substantial differences among current SOA schemes highlight a lack of consensus within the air quality modelling community. Evaluating model simulation results using ambient measurements is unlikely to resolve these discrepancies because uncertainties in SOA formation and precursor emissions are deeply intertwined. The limitations of current SOA schemes should be recognized and

acknowledged because model choice can greatly influence predicted SOA concentrations and their evolution, ultimately impacting air quality forecasts, assessments, and regulatory decisions.

Keywords: Secondary organic aerosol (SOA), chemical transport model (CTM), two-product, volatility basis set (VBS), SOA yields, CAMx, CMAQ, GEOS-Chem, WRF-Chem, CHIMERE

1. Introduction

Organic Aerosol (OA) contributes a large fraction of fine particulate matter ($PM_{2.5}$) due to primary OA emissions (POA) and the formation of secondary OA (SOA) from anthropogenic, biogenic, and biomass burning sources (Donahue et al., 2006; Huang et al., 2014; Tsimpidi et al., 2016). SOA precursor emissions include traditional volatile organic compounds (VOC) as well as non-traditional intermediate and semi-volatile VOC (IVOC and SVOC, respectively) whereas POA are directly emitted from combustion sources. Recent studies report that volatile chemical products (VCPs) are increasingly important contributors to SOA formation (Pennington et al., 2021; Sasidharan et al., 2023). Chemical transport models (CTMs) are essential tools for understanding the sources and transport of OA as well as assessing the effectiveness of mitigation strategies (e.g. Pye et al., 2021; Chang et al., 2022; Chen et al., 2024; Pennington et al., 2024; Vitali et al., 2024). However, accurately modeling SOA formation in CTMs has posed persistent challenges due to the intricate nature of SOA formation processes (Li et al., 2023). Scientific understanding of SOA formation pathways is continuously evolving. Therefore, it is crucial to review the state of science on SOA formation implemented in different CTMs and identify existing knowledge gaps.

In general, CTMs adopt one of two approaches for SOA simulation: the two-product scheme (Figure 1~~Figure 1(Figure 1)~~) or the volatility basis set (VBS) scheme (Figure 2~~Figure 2(Figure 2aa~~). Two-product schemes apply the absorptive gas-particle partitioning theory of Pankow (1994) using only two surrogate products to represent all of the condensable gases (CGs) formed when SOA precursors are oxidized in the gas

phase by OH radical, ozone (O_3), or NO_3 radical, e.g.:

$$\text{SOA precursor} + \text{OH} \rightarrow \alpha_1 \times \text{CG1} + \alpha_2 \times \text{CG2} \qquad \text{R1}$$

where CG1 and CG2 have different saturation concentration (C*); α_1 and α_2 are molar stoichiometric yields. The α and C* values for CG1 and CG2 are fitted to SOA formation observed in chamber experiments. SOA formation depends on the total amount of OA present (Pankow, 1994) and consequently SOA formation depends on POA. POA is usually treated as non-volatile in two-product schemes (e.g., Strader et al., 1999; Schell et al., 2001) but can be treated as semi-volatile in a modified two-product scheme (e.g. Huang et al. 2024).

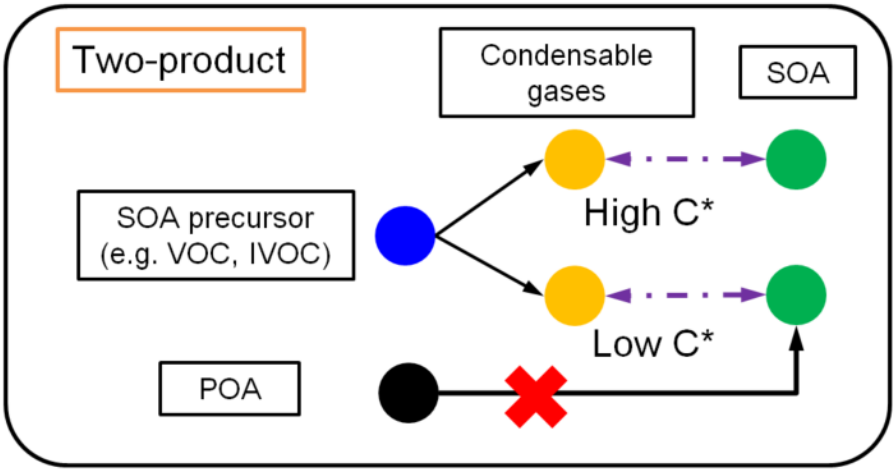

Figure 1 Illustration of a "two-product" SOA scheme combined with a non-volatile treatment of POA

The VBS framework (Donahue et al., 2006) expands the two-product model by having more condensable gases that are systematically organized by volatility (i.e., C^*). Condensable organic compounds are categorized based on their volatility into bins that are typically separated by a factor of 10, e.g., four bin with C^* of 1, 10, 100, 1000 μg/m^3:

$$\text{SOA precursor} + \text{OH} \rightarrow \alpha_1 \times \text{CG}|_{C^*=1} + \alpha_2\ \text{CG}|_{C^*=10} + \alpha_3 \times \text{CG}|_{C^*=100} + \alpha_4 \times \text{CG}|_{C^*=1000} \qquad \text{R2}$$

Similar to the two-product model, the VBS framework is based on the absorptive partitioning theory and the CG yield (α) for each volatility bin can be obtained by fitting the results of laboratory studies. Many VBS schemes treat POA as being semi-volatile and able to dynamically partition between the gas and particle phase depending on environmental factors, similar to SOA. Figure 2~~Figure 2~~~~Figure 2~~ illustrates the "1-

dimensional" (1-D) VBS framework where volatility is the dimension that varies (discretized to volatility bins) and panels a-d illustrate various treatments of SOA aging. In the 2-D VBS introduced by Donahue et al. (2011), both volatility and oxidation state can vary independently. The 1.5-D VBS introduced by Koo et al. (2014) represents variations in volatility and oxidation state as a single coordinate by assuming they are related.

Figure 2~~Figure 2~~Figure 2a~~a~~ depicts a four-bin VBS framework with no aging of OA after the initial formation of SOA. Emitted SOA precursors (e.g., VOC, IVOC) undergo initial gas-phase oxidation and produce four types of CGs which can immediately condense to form SOA. Beyond initial oxidation, multi-generational aging processes can occur and include functionalization and/or fragmentation of gas-phase CGs, oligomerization of condensed-phase SOA, SOA photolysis, and heterogeneous SOA oxidation. Functionalization and oligomerization typically increase SOA mass by lowering volatility, whereas fragmentation and photolysis decrease SOA mass. Figure 2~~Figure 2~~Figure 2b~~b~~ depicts a VBS framework incorporating a step-wise OH-oxidation functionalization process as included in many VBS schemes, where CGs undergo gas-phase reactions (usually parameterized as OH-oxidation) that add oxygen-containing functional groups and successively lower volatility. This functionalization increases molecular weight with each oxidation generation, which can be parameterized as a percentage increase (usually 7.5% or 15%) to account for added oxygen (Robinson et al., 2007; Shrivastava et al., 2015). Gas-phase reactions of CGs can cause molecular fragmentation as well as functionalization. As SOA ages, fragmentation reactions may gain significance (Cappa et al. 2012). Figure 2~~Figure 2~~Figure 2c~~c~~ shows a VBS framework with both functionalization and fragmentation. In this scheme, OH-oxidation of the CGs forms products across lower (due to functionalization) and higher (due to fragmentation) volatility bins that are often parameterized using predefined fractions. Particle-phase oligomerization, as illustrated by Figure 2~~Figure 2~~Figure 2d~~d~~, is another SOA aging process where condensed SOA molecules join together and form larger SOA molecules with extremely low volatility. Some schemes refer to

oligomerization as polymerization. Typically, the rate of oligomerization is modeled as independent of the gas-phase oxidant level.

Given the diverse treatments of SOA formation employed in CTMs, it is both necessary and important to comprehensively understand and quantify the similarities and differences among schemes/models. Direct comparisons of simulated SOA concentrations across different CTMs can be both time-consuming and resource-intensive. Furthermore, variations in other model configurations, such as physical processes, may obscure the distinctions associated with the SOA schemes themselves. To address this issue, we performed offline calculations outside the selected CTMs to focus on SOA formation and aging processes, as described in Section 2. Details of each SOA model/scheme reviewed are presented in Section 3. Section 4 provides a comparative analysis of ~~initial (i.e.~~the non-aged~~)~~ SOA yields from typical precursors as simulated by each model/scheme. Furthermore, we explore how SOA aging is treated by different schemes and how NO*x* conditions impact SOA yields. Results from this study underscore the variability in SOA yields and highlight the need for careful consideration of model selection and application in the context of air quality studies.

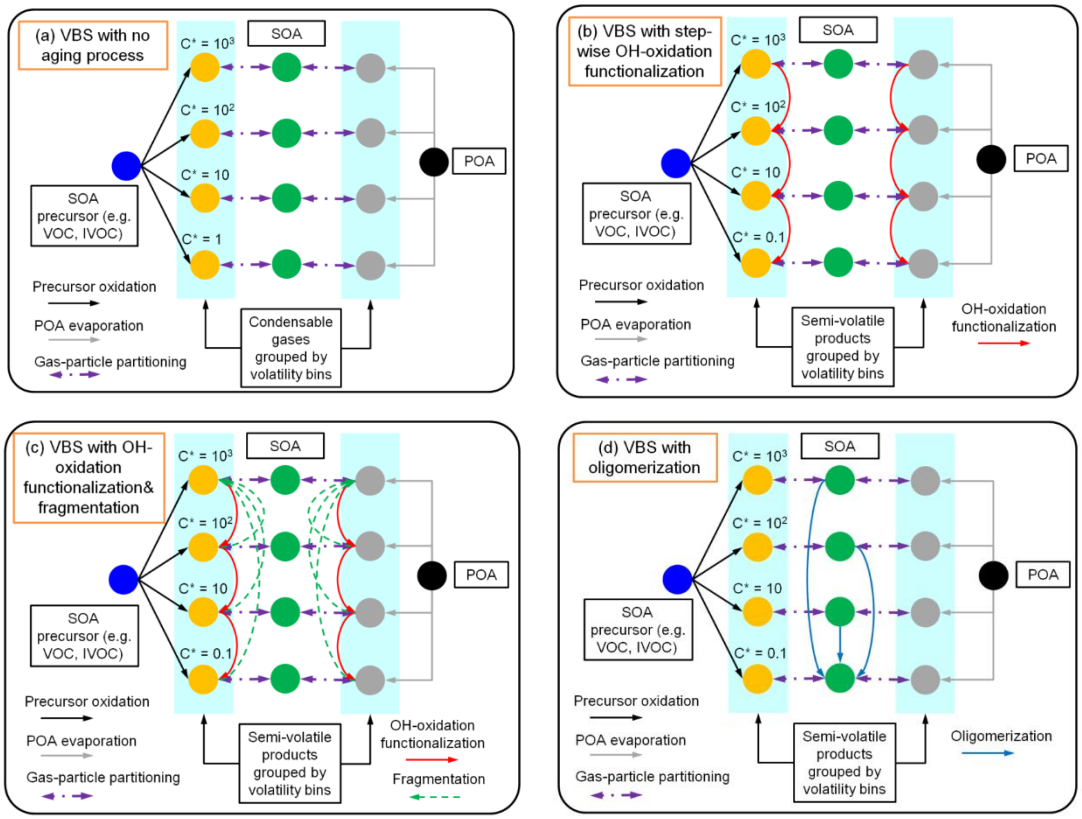

Figure 2 Illustration of VBS schemes with alternative treatments of aging: (a) no aging; (b) with step-wise OH oxidation causing functionalization only; (c) with OH-oxidation causing both functionalization and fragmentation; and (d) with condensed-phase oligomerization.

2. Methods

2.1 CTMs and SOA schemes reviewed

To understand the current state of SOA modelling in CTMs, we reviewed schemes implemented in several regional models that are used in the U.S., Europe, and Asia as well as one global model. We review eight SOA schemes implemented in five models, namely the Comprehensive Air Quality with Extensions (CAMx, https://www.camx.com/, accessed on Feb 15th, 2024), the Community Multiscale Air Quality (CMAQ, https://github.com/USEPA/CMAQ/, accessed on Feb 15th, 2024), GEOS-Chem (https://geos-chem.readthedocs.io/en/stable/, accessed on Feb 15th, 2024), WRF-Chem (https://ruc.noaa.gov/wrf/wrf-chem/, accessed on Feb 15th, 2024), and CHIMERE (https://www.lmd.polytechnique.fr/chimere/docs/, accessed on Feb 15th, 2024). For each model/scheme (hereafter "scheme" for simplicity), we reviewed the official documentation (e.g., user's guide), peer-reviewed publications, and, in some cases, the model source code to understand each SOA parameterization and gather parameter data. A comparative overview of the SOA schemes is presented in Table 1~~Table 1Most schemes consider SOA formation from anthropogenic VOC (AVOC), IVOC, and biogenic VOC (BVOC). Some schemes also account for the impact of sunlight exposure and/or atmospheric oxidation on SOA formation/destruction, which is generally referred to as "SOA aging". Table S1 provides general information for each SOA model/scheme with more detailed information presented in Section 3~~ while comprehensive details regarding their specific parameterizations can be found in Section S1 of the Supporting Information.

The review of these SOA schemes reveals diverse parameterizations ranging from simplified, non-volatile assumptions to complex, multi-dimensional volatility basis sets. CAMx offers two distinct approaches: the SOAP2 scheme (based on Strader et al., 1999) and the 1.5-D VBS (Koo et al., 2014). SOAP2 has non-volatile POA and a two product

SOA scheme (Figure 1~~Figure 1~~) with yields fitted to the aged VBS scheme of Hodzic et al. (2016), effectively treating aging as implicit. The 1.5-D VBS treats POA as semi-volatile and explicitly models gas-phase aging for anthropogenic and intermediate volatility precursors via OH-oxidation (Figure 2~~Figure 2~~b), although this stepwise aging is disabled for biogenic precursors to prevent aerosol mass overprediction. The CMAQ model also provides alternative schemes: the established AERO7 scheme (Appel et al., 2021) and the newer CRACMM scheme (Pye et al., 2023). AERO7 utilizes a 1-D VBS framework for POA and SOA that incorporates aging primarily through particle-phase processes (Figure 2~~Figure 2~~d), specifically the oligomerization of anthropogenic and biogenic precursors and the hydrolysis of organic nitrates derived from monoterpenes. CRACMM also utilizes a 1-D VBS framework for POA and SOA and simulates aging through sequential gas-phase oxidation reactions involving functionalization and/or fragmentation (Figure 2c; Pye et al., 2023). GEOS-Chem includes a "Simple" scheme that treats SOA as non-volatile with fixed yields that are linked to ambient measurements, alongside a "Complex" 1-D VBS scheme without additional aging processes (Figure 2a; Pai et al., 2020). CHIMERE's 1-D VBS scheme is notable for its comprehensive aging scheme with functionalization, fragmentation, and oligomerization (Figure 2d) where oxidation products are redistributed across volatility bins (CHIMERE, 2023). The WRF-Chem MOSAIC scheme employs a 1-D VBS for most VOCs but applies a specific stepwise gas-phase aging mechanism exclusively to IVOCs (Shrivastava et al. 2011).

Despite these structural differences, the schemes share foundational similarities, particularly in the reliance on absorptive partitioning theory by most schemes. With the exception of the GEOS-Chem Simple scheme, which assumes irreversible condensation, all models utilize either a two-product or VBS framework to describe the equilibrium partitioning of semi-volatile organic compounds. However, the treatment of aging remains the most significant source of divergence. Approaches vary from neglecting aging entirely (GEOS-Chem Complex, CAMx SOAP2) to implementing distinct mechanisms such as gas-phase oxidation (CAMx VBS, CMAQ CRACMM)

versus particle-phase oligomerization (CMAQ AERO7). Additionally, the representation of IVOCs varies substantially, ranging from omission from the GEOS-Chem Simple scheme, a single lumped IVOC in most schemes, and several lumped IVOCs in the CRACMM scheme.

2.2 Offline calculation of ~~initial~~non-aged SOA yields

The direct comparison of simulated SOA concentrations across different schemes through conducting full simulations is time-consuming and uncertain because configuring all models consistently is challenging. Furthermore, differences in the non-SOA physical and chemical processes between models may obscure the distinctions attributable specifically to the SOA schemes themselves. To address this issue, an offline calculation (Huang et al., 2023, 2024) is employed to compare the ~~initial~~non-aged SOA yield (i.e., prior to any aging effects) associated with different precursors across various schemes. For a two-product scheme, the ~~initial~~non-aged SOA yield (Y) is calculated by combing the gas-particle partitioning theory with the stoichiometric coefficients α_i:

$$Y = \frac{\alpha_1}{1 + C_1^*/C_{OA}} + \frac{\alpha_2}{1 + C_2^*/C_{OA}} \quad \text{Eq. 1}$$

where C_{OA} is the total ambient concentration of organic compounds (i.e., POA + SOA) and α_1, α_2, C_1^*, and C_2^* represent the stoichiometric coefficients and the effective saturation concentrations of the above two products, which is obtained by fitting the results of laboratory studies. Similarly, for a four-bin VBS scheme with no aging effects ~~(e.g. Figure 2a),~~ the SOA yield is calculated as:

$$Y = \frac{\alpha_1}{1 + 1/C_{OA}} + \frac{\alpha_2}{1 + 10/C_{OA}} + \frac{\alpha_3}{1 + 100/C_{OA}} + \frac{\alpha_4}{1 + 1000/C_{OA}} \quad \text{Eq. 2}$$

where α_i is the ~~initial~~non-aged oxidation yield for each volatility bin i (i=1,2,3,4). Utilizing either Eq. 1~~Eq. 1~~ or Eq. 2~~Eq. 2~~, the SOA yields under high- and low-NOx conditions can be determined at 298 K and total OA concentrations ranging from 0.1 μg/m^3 to 50 μg/m^3, using the stoichiometric coefficients provided by each scheme (~~listed~~see detailed parameters in Section S1 of the Supporting Information).

Table 1 Summary of SOA schemes implemented in CTMs reviewed in this study[a]

Model (version)	SOA scheme	SOA precursors	Aging treatment	POA treatment	SOA photolysis	References
CAMx v7.20	SOAP2	BENZ/TOL/XYL ISOP/TERP/SESQ IVOC	No aging effect	Non-volatile, no further reactions	Photolysis rate parameterized as 0.1% of the NO_2 photolysis rate (J_{NO2}).	Ramboll (2022) Koo et al. (2014)
	1.5D VBS		Gas-phase OH-oxidation aging for SOA formation from AVOC and IVOC	Semivolatile; gas-phase undergoes further oxidation		
CMAQ v5.4	AERO7	BENZ/TOL/XYL ISOP/TERP/SESQ IVOC	Particle-phase of semivolatile products forms oligomers; products generated by TERP + NO_3 undergo hydrolysis to form low-volatile products.	Semivolatile; gas-phase undergoes further oxidation	N/A	https://github.com/USEPA/CMAQ
	CRACMM	BENZ/TOL/XYM/XYE APIN/LIM/SESQ IEPOX IVOC	OH oxidation aging resulting in functionalization and fragmentation based on modified 2-D VBS framework	Semivolatile; gas-phase undergoes further oxidation	N/A	Pye et al. (2023)
GEOS-Chem v14.3.0	Simple	ISOP/TERP/SESQ Anthropogenic precursor scaled based on CO emissions	No aging effect	Non-volatile; 50% of POA is directly emitted; 50% is formed with a lifetime of 1.15 days, without dependence on local oxidation levels.	Described in literature but not found in source code	Pai et al. (2020), Pye et al. (2010) https://geos-chem.readthedocs.io/en/stable/
	Complex	BENZ/TOL/XYL IVOC ISOP/MTPO LIMO/SESQ		Semivolatile; gas-phase undergoes further oxidation with OH to form oxidized POA with lower volatility.		

Model (version)	SOA scheme	SOA precursors	Aging treatment	POA treatment	SOA photolysis	References
CHIMERE v2023	VBS	ARO1/ARO2 ALK4/ALK5 OLE1/OLE2 IVOC ISOP/TERP/HUMULE	OH oxidation aging with both functionalization and fragmentation; aerosol phase undergoes oligomerization to form non-volatile products.	Semivolatile; gas-phase undergoes further oxidation.	N/A	Zhang et al. (2013); Shrivastava et al. (2015); Couvidat et al. (2018); CHIMERE (2023)
WRF-Chem v4.4	MOSAIC	ALK4/ALK5 ARO1/ARO2 OLE1/OLE2 IVOC ISOP/TERP/SESQ	No aging for AVOC and BVOC; gas-phase OH-oxidation of IVOC with 15% of mass added for each generation; no fragmentation.	Semivolatile; gas-phase undergoes further oxidation	Described in literature (Zawadowicz et al. 2020) but turned off in source code	Shrivastava et al. (2011)

~~S2-S9).~~ [a] See abbreviations in Supporting Information

The ~~initial~~non-aged SOA yield Y is always calculated as mass-based in this study while the stoichiometric coefficients α_i could either be expressed in mass-base (g/g) or molar-base (ppm/ppm). An illustrative calculation is provided in the Section of S2 of the Supporting Information, with calculation spreadsheet publicly available (see Data Availability section). The ~~initial~~non-aged SOA yields for CMAQ CRACMM are calculated slightly differently (details presented in Section ~~3.2.2~~S3 of the Supporting Information), given its special treatment of partially combining gas-phase chemistry and SOA formation. Our analysis included calculations for anthropogenic precursors (benzene, toluene, and xylene), IVOC and biogenic precursors (isoprene, monoterpene, and sesquiterpenes).

2.3 The effect of SOA aging

Some schemes, such as CAMx two-product and GEOS-Chem Simple, do not account for SOA aging while others adopt varying approaches to represent the aging process (for a comprehensive discussion, refer to Section 3). For schemes that include aging effects, we calculated the aged SOA yields for each precursor at a given time *t* by summing over the particle fraction of all the relevant volatility bins (*i*) using Eq. 3~~Eq. 3~~:

$$\text{Aged SOA yields}|_t = \sum_n \left(f^i_{particle} \cdot \text{SOA mass}|^i_t\right) \quad \text{Eq. 3}$$

where $f^i_{particle}$ is the particle-phase fraction of each volatility bin (calculated based on Eq. 4~~Eq. 4~~) and $\text{SOA mass}|^i_t$ is the bin total SOA mass (gas-phase + particle-phase) at time *t*; *n* is the total number of bins.

$$f^i_{particle} = \frac{1}{1 + C^*_i / C_{OA}} \quad \text{Eq. 4}$$

For gas-phase OH-oxidation style aging (e.g., Figure 2~~Figure 2~~b and 2c), the SOA mass is stepped through time ($\Delta t = t - (t\text{-}1)$) as follows:

$$\text{SOA mass}|^i_t = \text{SOA mass}|^i_{t\text{-}1} \times \left(f^i_{particle} + f^i_{gas} \cdot e^{-k_{OH}*[OH]*\Delta t}\right) + \sum_n \left[\text{SOA mass}|^k_{t\text{-}1} \times f^k_{gas} \cdot (1 - e^{-k_{OH}*[OH]*\Delta t}) \times \alpha^i_k\right] \quad \text{Eq. 5}$$

The first term on the right hand side is the SOA mass in volatility bin (*i*) from the previous time step (*t-1*) multiplied by the fractions that remain after Δt in the particle-phase ($f^i_{particle}$) and

gas-phase ($f^i_{gas} \cdot e^{-k_{OH}*[OH]*\Delta t}$; $f^i_{gas} = 1 - f^i_{particle}$) considering OH-oxidation. The second term is the SOA mass gain from OH-oxidation summed across all *n* volatility bins. Here, α^i_k is the mass yield coefficient from bin *k* to bin *i* and the term $f^k_{gas} \cdot (1\text{-}e^{-k_{OH}*[OH]*\Delta t})$ is the gas-phase fraction of SOA in bin *k* oxidized by OH during Δ*t*.

For particle-phase oligomerization-style aging (e.g. Figure 2~~Figure 2~~d and the CMAQ AERO7 scheme), the aged SOA yield includes the mass of a non-reactive and non-volatile oligomer bin (OLIG) in addition to the semi-volatile bins:

$$\text{Aged SOA yield}|_t = \sum_n (f^i_{particle} \cdot \text{SOA mass}|^i_t) + \text{SOA mass}|^{OLIG}_t \quad \text{Eq. 6}$$

The SOA mass (gas-phase + particle-phase) in each volatility bin (*i*) steps through time following Eq. 7~~Eq. 7~~ and the mass of the non-volatile oligomer bin ($\text{SOA mass}|^{OLIG}_t$) grows with mass-transfer from semi-volatile bins according to Eq. 8~~Eq. 8~~:

$$\text{SOA mass}|^i_t = \text{SOA mass}|^i_{t-1} \times (f^i_{gas} + f^i_{particle} \cdot e^{-k_{OLIG}*\Delta t}) \quad \text{Eq. 7}$$

$$\text{SOA mass}|^{OLIG}_t = \text{SOA mass}|^{OLIG}_{t-1} + \sum_n \{\text{SOA mass}|^i_{t-1} \cdot f^i_{particle} \cdot (1 - e^{-k_{OLIG}*\Delta t}) \cdot \beta^i\} \quad \text{Eq. 8}$$

k_{OLIG} is the oligomerization rate and β^i is the mass yield coefficient from bin *i* to the non-volatile bin OLIG.

To compare the aging effects of different schemes, we applied Eq. 3~~Eq. 3~~ to Eq. 8~~Eq. 8~~ for one day of aging with an OH concentration of 3×10^6 molecules/cm^3 with k_{OH} and/or k_{OLIG} for each scheme when applicable. A time step (Δt) of 0.2 hr was used. Any additional calculations and assumptions associated with each scheme are further described below.

~~3. Parameterization of SOA scheme in different CTMs~~

~~3.1 CAMx~~

2.4 ~~The Comprehensive Air quality Model with Extensions (CAMx; Emery et al., 2024) is an Eulerian CTM developed and distributed by Ramboll and version 7.20 was released on May 2nd, 2022 (https://www.camx.com/, accessed on Feb 15th, 2024). CAMx provides two options to simulate SOA chemistry/partitioning: a "two-product" semi-volatile equilibrium scheme called SOAP (Strader et al., 1999) and a hybrid 1.5-dimension volatility basis set (1.5-D VBS) approach~~Box model tests based on different SOA schemes

We implemented three updated SOA schemes in CAMx and performed 2-layer box modeling of two locations with varied anthropogenic emissions to quantify how differences between schemes can influence predicted SOA concentrations and their response to emission changes. The alternate SOA schemes use the existing CAMx SOAP2 code with updated SOA yield parameters so that model results clearly depend on yield assumptions rather than scheme formulation or coding. Two regions of Texas were selected to capture contrasting emission environments: Dallas-Fort Worth (DFW), a major urban area dominated by anthropogenic emissions (e.g., aromatics and IVOCs), and Tyler (TYL), a rural area in Northeast Texas characterized by high biogenic activity. The box model has a surface layer and a residual layer with time-varying surface layer depth to provide a simple representation of pollutant accumulation, carry-over, and diurnal variation. Simulations were conducted over a 5-day period, utilizing meteorological inputs and initial conditions derived from the Texas Commission on Environmental Quality (TCEQ) 2019 3-D CAMx modeling platform (TCEQ, 2022).

We implemented three new SOA schemes into CAMx that emulate SOA yields produced by the CMAQ AERO7, CMAQ CRACMM and Simple schemes. Each scheme was implemented by updating the yield parameters used by the CAMx SOAP2 scheme. For the CMAQ AERO7 and CRACMM schemes, yield curves were fitted to the respective data (Figure S3) for each SOA precursor. These yields were mapped to the volatility bins defined by CAMx SOAP2 to obtain the corresponding molar-based stoichiometric coefficients (Table S11-S14). Like the GEOS-Chem Simple scheme, the CAMx Simple scheme treats SOA as non-volatile with fixed

yields that are based on multi-model averages and work by Seltzer et al. (2021). Detailed descriptions of the fitting procedures, updated Simple yields, and box model configurations are provided in the Section S3 of the Supporting Information.

We further investigate the response of SOA concentrations to varying anthropogenic VOC and NO*x* emissions by performing a matrix of 100 simulations for each location and SOA scheme. This approach allows for a comparison of scheme performance across a wider range of atmospheric concentrations and VOC/NO*x* ratios. Anthropogenic emissions in the sensitivity runs were based on weekday rates, while the biogenic emissions remained unscaled and varied by date, consistent with the base case simulations. Anthropogenic VOC emissions were scaled from 0.1 to 1.0 (in increments of 0.1), while anthropogenic NO*x* emissions were scaled from 0 to 9 (in increments of 1) which caused oxidant production to transition between NO-limited and VOC-limited conditions. An additional simulation with a 50% reduction in NO*x* emissions was conducted to examine SOA response to NO*x* abatement, which is a critical consideration for current and future air quality planning.

~~(Koo et al., 2014).~~ ~~The former is compatible with advanced probing tools, including the Particulate Source Apportionment Technology (PSAT) and the decoupled direct method (DDM), while the latter is not.~~

~~3.1.1 CAMx SOAP2~~

~~In the CAMx SOAP scheme version 2 (SOAP2), POA is treated as non-volatile and does not chemically evolve. SOA formation is represented by a modified "two product" model described above (), where gas-phase VOC and IVOC are oxidized to CGs that can condense to SOA. SOAP2 modifies the two-product scheme by adding a third product, which is considered non-volatile and always condenses to SOA. The CG products from anthropogenic and biogenic precursors have different volatilities in SOAP2. Thus, SOAP2 includes 6 product species overall, as shown in Table S2. The SOA mass yields do not differentiate between different oxidants (i.e., OH, O_3, and NO_3) in SOAP2 and the yield coefficients are fitted to aged SOA yields (Hodzic et al., 2016). Therefore, no further aging is included in SOAP2. However, SOA is destroyed in the particle phase by photolysis at a rate of 0.1%×J_{NO2} (NO_2 photolysis rate).~~

Aqueous-phase formation of non-volatile SOA from glyoxal and methylglyoxal is also included with SOAP2.

3.1.2 CAMx VBS

The CAMx hybrid VBS approach, called 1.5-D VBS, combines the simplicity of 1-D VBS (Donahue et al. 2006; Robinson et al. 2007) with the ability to describe the evolution of OA in both dimensions of oxidation state and volatility (Koo et al. 2014). Unlike SOAP2, CAMx 1.5-D VBS treats POA as semi-volatile, and uses two basis sets with five volatility bins (C* ranging from 10^{-1} to 10^{3} $\mu g/m^3$ at 298K) to describe SOA formation from anthropogenic and biogenic precursors, respectively. Gas-phase oxidation products in different bins are continuously oxidized by OH (with a rate constant k_{OH} of 2×10^{-11} cm^3 $molecule^{-1}s^{-1}$) that move mass from higher volatility bins to the next lower volatility bin in a step-wise manner (for example, from C*=1000 $\mu g/m^3$ to C*=100 $\mu g/m^3$ and from C*=100 $\mu g/m^3$ to C*=10 $\mu g/m^3$, as illustrated by Figure 2b). For biogenic SOA, this step-wise aging is disabled because over-prediction of OA in rural areas was reported (Lane et al., 2008; Murphy and Pandis, 2009). Like SOAP2, SOA is destroyed by particle-phase photolysis at a rate of $0.1\%\times J_{NO2}$. Table S3 shows the parameters used for the CAMx 1.5-D VBS scheme. The SOA yields from NO_3-initiated monoterpene oxidation are different from OH-initiated oxidation and the SOA yields for monoterpenes and IVOC are NO*x* independent. CAMx 1.5-D VBS differentiates SOA yields from different IVOC sources: gasoline engines (IVOG), diesel engines (IVOD), biomass burning (IVOB), and other anthropogenic sources (IVOA). SOA yields for IVOD, IVOB and IVOA are the same and we only present results for IVOA in this study. Aqueous-phase formation of non-volatile SOA from glyoxal and methylglyoxal is also included in the CAMx 1.5D VBS.

3.2 CMAQ

The Community Multiscale Air Quality (CMAQ) model is developed and distributed by the US Environmental Protection Agency (EPA). The version CMAQ v5.4 released in October 2022 offers three SOA options: AERO7 inherited from earlier versions (Appel et al., 2021), CRACMM (Pye et al., 2023) introduced in v5.4 for the first time, and a 2D-VBS developed by Tsinghua University (, accessed Feb 15th, 2024). We reviewed the first two schemes because both were developed by EPA to support air quality planning in the U.S. and elsewhere.

3.2.1 CMAQ AERO7

The CMAQ AERO7 introduced in version 5.3 (Appel et al. 2021) tracks SOA formation from anthropogenic VOC (benzene, alkanes, aromatics, polycyclic aromatic hydrocarbons (PAHs)), biogenic VOC (isoprene, α-pinene, monoterpenes, and sesquiterpenes), and IVOC. Additionally, AERO7 accounts for in-cloud SOA formation from glyoxal and methylglyoxal and aerosol aqueous-phase SOA formation from glyoxal, methylglyoxal and isoprene epoxydiols (IEPOX). AERO7 scheme employs VBS based approaches to represent SOA yields from different precursors, with varying volatility ranges for each precursor. Table S4 to Table S6 list the AERO7 SOA yields for precursors considered in this study. Specifically, AERO7 uses a VBS approach with four bins (C^* ranging from 0.01 $\mu g/m^3$ to 100 $\mu g/m^3$ at 298K, Table S4) to represent SOA formation from anthropogenic VOC precursors (e.g., benzene, long alkanes, PAHs) and seven bins (C^* ranging from 0.01 to 10^7 $\mu g/m^3$ at 298K, Table S5) for α-pinene and monoterpenes. Isoprene and sesquiterpene oxidation products are parameterized with two and one semivolatile products (Table S6), respectively. IVOC in CMAQ is represented by model species pcVOC, which oxidizes with OH to form a low-volatility condensable vapor (pcSOG, $C^*=10^{-5}$ $\mu g/m^3$) with a molar yield of 1 (Murphy et al. 2017, Table S6).

AERO7 incorporates aging treatments for SOA that vary by precursor as detailed in Table S10. SOA formed from AVOC, isoprene, and sesquiterpenes undergo oligomerization in the particle-phase to form non-volatile SOA (as illustrated by Figure 2d) with a static rate constant k_{OLIG} of 9.49×10^{-6} s^{-1} (equivalent to a lifetime of ~30 hr). In contrast, no oligomerization occurs for SOA formed from OH-initiated monoterpene oxidation, while SOA formed from NO_3-initiated monoterpene oxidation is subject to particle-phase hydrolysis to non-volatile SOA with a rate constant of 9.25×10^{-5} s^{-1} (equivalent to a lifetime of 3 hr). Unlike CAMx, SOA photolysis is not considered in AERO7.

3.2.2 CMAQ CRACMM

The Community Regional Atmospheric Chemistry Multiphase Mechanism (CRACMM) was introduced in CMAQv5.4 (Pye et al., 2023). Unlike other SOA schemes, CRACMM partially integrates CG formation and CG aging with oxidant formation in the gas-phase chemical

mechanism. Consequently, SOA formation occurs through multiple sequential reactions (as illustrated below for benzene), meaning that the SOA yield parameters are too complex to be tabulated for CRACMM in contrast to the other schemes reviewed here. CRACMM SOA formation considers a comprehensive range of reactive organic carbon (ROC) precursors, including alkane-like ROC, aromatics, furans, isoprene, monoterpenes, sesquiterpenes, glyoxal and methylglyoxal. Furthermore, CRACMM categorizes IVOC based on functional groups to aromatic IVOC, oxygenated IVOC, and alkane IVOC. Aqueous SOA formation from IEPOX, glyoxal, and methylglyoxal follow CMAQ AERO7.

SOA formation from the OH-initiated oxidation of benzene (BENZ in CRACMM) is shown here as an example where only the SOA-related products are identified (to):

$$\text{BENZ} + \text{OH} \rightarrow 0.470\ \text{BENP} + 0.530\ \text{PHEN} + \ldots \quad \text{R3}$$

$$\text{BENP} + \text{NO} \rightarrow 0.001\ \text{VROCP4OXY2} + 0.001\ \text{VROCN1OXY6} + 0.499\ \text{FURANONE} + \ldots \quad \text{R4}$$

$$\text{BENP} + \text{HO2} \rightarrow 0.398\ \text{VROCN1OXY6} + \ldots \quad \text{R5}$$

$$\text{FURANONE} + \text{OH} \rightarrow 0.040\ \text{ASOATJ} + \ldots \quad \text{R6}$$

$$\text{PHEN} + \text{OH} \rightarrow 0.152\ \text{ASOATJ} + \ldots \quad \text{R7}$$

Non-volatile products (e.g. ASOATJ in this example) always form 100% SOA. In contrast, semi-volatile products (e.g. VROCP4OXY2 and VROCN1OXY6) can react further with OH in the gas-phase and undergo functionalization and/or fragmentation within a simplified 2-D VBS. By employing a straightforward application of linear algebra, we can multiply the stoichiometric coefficients of sequential reaction steps (i.e., to for benzene) under both high and low NO*x* conditions. This approach results in SOA yields that align closely with the values of Pye et al. (2023) for the average of high and low NO*x* conditions. However, this algebraic calculation assumes 100% reaction of the precursor and all intermediate products, such as phenol (PHEN) and furanone. In reality, intermediate products react sequentially with varying reaction rates (e.g., R3 to R7) that are influenced by the concentrations of OH, HO_2 or NO. For illustration, we present detailed calculations of aged SOA formation for CRACMM benzene and α-pinene in Section S1. As shown by these calculations, the initial SOA yields in

CRACMM are zero and thus were excluded from the discussion of initial yields in Section 4.1. As the reactions progress, however, SOA yields begin to rise, demonstrating the importance of aging to CRACCM. Like CMAQ AERO7, SOA photolysis is not accounted for in CRACMM.

3.3 GEOS-Chem

GEOS-Chem is a global chemical transport model driven by meteorological input from the Goddard Earth Observing System (GEOS) of the NASA Global Modeling and Assimilation Office (, accessed on March 1st, 2024). GEOS-Chem is widely used for studying air quality and atmospheric chemistry. Two SOA schemes are available within GEOS-Chem: a simple scheme and a complex scheme (hereafter GEOS-Chem Simple and GEOS-Chem Complex) as described by Pai et al. (2020). The former provides computationally efficient SOA estimates by treating all SOA as non-volatile and using anthropogenic CO emissions as a surrogate for all anthropogenic SOA precursor emissions. The latter implements a conventional 1-D VBS framework. The GEOS-Chem Simple scheme is interesting because it has been shown to replicate atmospheric measurements more successfully than complex schemes with many more parameters (Nault et al., 2021).

3.3.1 GEOS-Chem Simple scheme

The GEOS-Chem Simple scheme converts a single lumped anthropogenic SOA (ASOA) precursor to non-volatile SOA with a constant lifetime of 1 day and 100% yield. The anthropogenic precursor emissions are estimated using CO emissions as a proxy, with scaling factors of 1.3% and 6.9% for fire/biofuel and fossil fuel sources respectively. This scheme (Hodzic and Jimenez, 2011; Nault et al., 2021) was developed by comparing ambient measurements of SOA with CO, which confounds the assumed ASOA yield (100%) with the derived anthropogenic precursor emission scaling factors (1.3% or 6.9%). Consequently, we exclude the Simple scheme ASOA yields from some comparisons with other schemes presented below because the assumption of 100% yield could be considered arbitrary. SOA formation from IVOC is not explicitly considered in the GEOS-Chem Simple scheme. For BVOC, the Simple scheme assumes formation of non-volatile biogenic SOA (BSOA) with constant yields of 3% for isoprene and 10% for monoterpenes and sesquiterpenes. 50% of the

BSOA is formed promptly and the remaining 50% is formed with a constant lifetime of 1.15 days. The Simple scheme has no treatment of SOA aging or SOA photolysis.

3.3.2 GEOS-Chem Complex scheme

The GEOS-Chem complex scheme represents SOA formation from anthropogenic and biogenic precursors using a VBS framework. The SOA yields from OH and O_3 initiated oxidation are listed in Table S7 (Pye et al., 2010). This scheme does not include further aging processes (e.g. a) and our review of the source code found no treatment of SOA photolysis. SOA formation from IVOC is simulated using naphthalene as a proxy. Additionally, irreversible SOA formation occurs from the aqueous-phase reactive uptake of isoprene (Marais et al., 2016), which is outside the primary focus of the current study.

3.4 CHIMERE

CHIMERE is an Eulerian chemistry-transport model widely used for operational regional air quality forecasts (Honore et al. 2008) and research in Europe (Beekmann and Vautard, 2010; Sciare et al., 2010) as well as other regions of the world (Zhang et al., 2012; Hodzic et al., 2009, 2010; Ma et al., 2019). Version v2023r1 was released in December 2023. Within CHIMERE, three SOA formation schemes are available: single-step oxidation, the Hydrophilic/Hydrophobic Organics (H_2O) mechanism (Couvidat et al., 2018), and a VBS scheme (Zhang et al., 2013; Cholakian et al., 2018). The VBS scheme includes two subsets: one involving only functionalization and the other involving functionalization, fragmentation, and oligomerization (Zhang et al. 2013; Shrivastava et al. 2015).

We reviewed the CHIMERE VBS scheme with functionalization, fragmentation, and oligomerization processes, referred to as CHIMERE VBS. This scheme models SOA precursors using the SAPRC99 VOC lumping scheme (Luecken et al., 2008) and four VBS bins (C* ranging 1 to 10^3 $\mu g/m^3$ at 298K) with corresponding SOA mass yields listed in Table S8 (Zhang et al. 2013; CHIMERE, 2023). The aging processes for AVOC and BVOC are slightly different in CHIMERE VBS but basically follow c. For AVOC, the first two generations of gas-phase products undergo OH-initiated functionalization oxidation with a 7.5% mass gain to account for oxygen addition:

$$ASOA_n(g) + OH \rightarrow 1.075*ASOA_{n-1}(g) \qquad R8$$

Subsequent generations undergo both functionalization (15% yield adjusted for oxygen mass gain) and fragmentation (75%):

$$ASOA_n(g) + OH \rightarrow 0.16125*ASOA_{n-1}(g) + 0.75*ASOA_4(g) \quad R9$$

Subscript 4 represents the most volatile bin ($C^*=10^3$ µg/m^3 at 298K). Implicitly, assumes a 10% yield of volatile products such as CO or CO_2. For BVOC, the fragmentation process occurs from the first generation:

$$BSOA_n(g) + OH \rightarrow 0.16125*BSOA_{n-1}(g) + 0.75*BSOA_4(g) \quad R10$$

In the CHIMERE VBS scheme, both functionalization and fragmentation occur with an OH rate constant k_{OH} of 1×10^{-11} cm^3 molecule^{-1} s^{-1}. Non-volatile SOA (i.e., ANVSOA and BNVSOA) is formed by oligomerization with a rate constant k_{OLIG} of 3×10^{-4} s^{-1} corresponding to a lifetime of 1 hr (and).

$$ASOA_n(p) \rightarrow ANVSOA \quad R11$$

$$BSOA_n(p) \rightarrow BNVSOA \quad R12$$

CHIMERE represents IVOC using three high volatility bins of the POA VBS (POA7 to POA9, corresponding to $C^* = 10^4$ to 10^6 µg/m^3). The IVOC mass fraction assigned to each bin is 24%, 29%, and 47% (Zhang et al. 2013). The gas-phase fraction of each volatility bin undergoes OH-initiated oxidation to form oxidized POA (OPOA) with lower and/or higher volatility. Similar to ASOA formation, the first two generations of IV-SOA (SOA formed from IVOC) undergo only functionalization reactions (with a 7.5% mass gain,) while subsequent generations undergo both functionalization (15% goes to the next lower volatility bin) and fragmentation (75% goes to the next higher volatility bin,):

$$POA_n(g) + OH \rightarrow 1.075\ OPOA_{n-1}(g) \quad R13$$

$$POA_n(g) + OH \rightarrow 0.16125\ OPOA_{n-1}(g) + 0.75\ OPOA_{n+1}(g) \quad R14$$

3.5 WRF-Chem

WRF-Chem adds atmospheric chemistry to the Weather Research and Forecasting (WRF) meteorological model to simulate interactions between meteorology and atmospheric chemistry. Version v4.4 released in April 2022 offers five aerosol schemes (WRF-Chem, 2022): 1) Modal Aerosol Dynamics Model for Europe (MADE/SORGAM, Schell et al. 2001), 2) Modal Aerosol Dynamics Model for Europe with the VBS (MADE/VBS), 3) Modal Aerosol

~~Module (MAM), 4) Model for Simulating Aerosol Interactions and Chemistry (MOSAIC) sectional model aerosol parametrization, and 5) bulk aerosol module from GOCART.~~

~~We reviewed the MOSAIC scheme as an example of a VBS scheme with functionalization and fragmentation. In the MOSAIC scheme (Shrivastava et al. 2011), SOA formation from OH-oxidation is considered but reactions with O_3 and NO_3 radicals are not included. The formation of SOA from both AVOC and BVOC is modeled using a 4-bin VBS (C* ranging from 0.1 to 100 $\mu g/m^3$ at 298K) with constant yields (Table S9). No additional aging processes are considered for the condensable gases. SOA photolysis is included in the source code but turned off by default.~~

~~In WRF-Chem, IVOC is represented by three bins, with C^* ranging from 10^4 to 10^6 $\mu g/m^3$. The formation of SOA from IVOC involves OH oxidation of both the non-oxygen (with subscript c) and oxygen parts (with subscript o), with a first-order rate constant k_{OH} of 4×10^{-11} cm^3 $molecule^{-1}$ s^{-1}. For the non-oxygen part, oxidation results in formation of non-oxygen and oxygen parts (with 15% mass gain) with lower volatility (and). At the same time, the oxygen parts oxidize with OH and move to a lower volatility bin (and). Therefore, at any time both non-oxygen and oxygen parts move to successively lower volatility bins. The lowest volatility species ($C^* = 0.01$ $\mu g/m^3$) are assumed to be inert and have no fragmentation reactions.~~

3. Results

43.1 Comparison of ~~initial~~non-aged SOA yields

~~Initial~~Non-aged SOA mass yields (g/g) for all schemes (except CMAQ CRACMM) are summarized in Table 2~~Table 2~~~~Table 1. Initial~~. Non-aged refers to the yields immediately following precursor oxidation and before any subsequent SOA aging process. Since mass yields can vary with C_{OA}, we assume C_{OA} of 10 $\mu g/m^3$ in Table 2~~Table 2~~~~Table 1,~~, which is relevant to ambient air quality and often used as a reference C_{OA} for SOA yield comparisons. The ratio of maximum to minimum ~~initial~~non-aged SOA yields for a same precursor shows wide variations across different schemes, with the least variation (factor of 1.8) observed for monoterpene at low NO*x* conditions and over three orders of magnitude for IVOC (factor of 3715). These variations can become greater when C_{OA} is either increased or decreased from 10

$\mu g/m^3$ (as assumed for Table 2~~Table 2Table 1))~~ and when effects of aging processes on ~~initial~~non-aged yields are included (as shown in Section 4.2).

~~4~~3.1.1 ~~Initial~~Non-aged SOA yields from anthropogenic VOC

Figure 3~~Figure 3~~ shows how the ~~initial~~non-aged SOA mass yields depend on C_{OA} for three anthropogenic VOC (AVOC), namely benzene (BENZ), toluene (TOL), and xylene (XYL). For WRF-Chem and CHIMERE, the SOA yields for model species ARO1 are used to represent BENZ and TOL whereas those of ARO2 are used for XYL. As illustrated by Figure 3~~Figure 3~~, the SOA yields from aromatics generally increase with C_{OA}, except for GEOS-Chem Simple. The SOA yields become independent of C_{OA} when the product is treated as non-volatile as exemplified by the GEOS-Chem Simple scheme, which assumes constant SOA yields of 100% for all three precursors. Conversely, the SOA yields increase strongly with C_{OA} when the SOA is treated as semi-volatile. The CAMx SOAP2 scheme is an intermediate case with SOA yields increasing more gradually with C_{OA} than the CHIMERE scheme. CMAQ AERO7 and GEOS-Chem Complex predict almost identical SOA yields (due to close stoichiometric coefficients) and exhibit no dependence on C_{OA} under low NO*x* conditions. Overall, schemes consistently show higher ASOA yields from aromatics under low NO*x* than high NO*x* conditions but diverge in the magnitude of these yields (max./min. yields at 10 $\mu g/m^3$ ranging from 2.0 to 5.8) and diverge in how yields depend on C_{OA} (ranging from independent to strongly increasing).

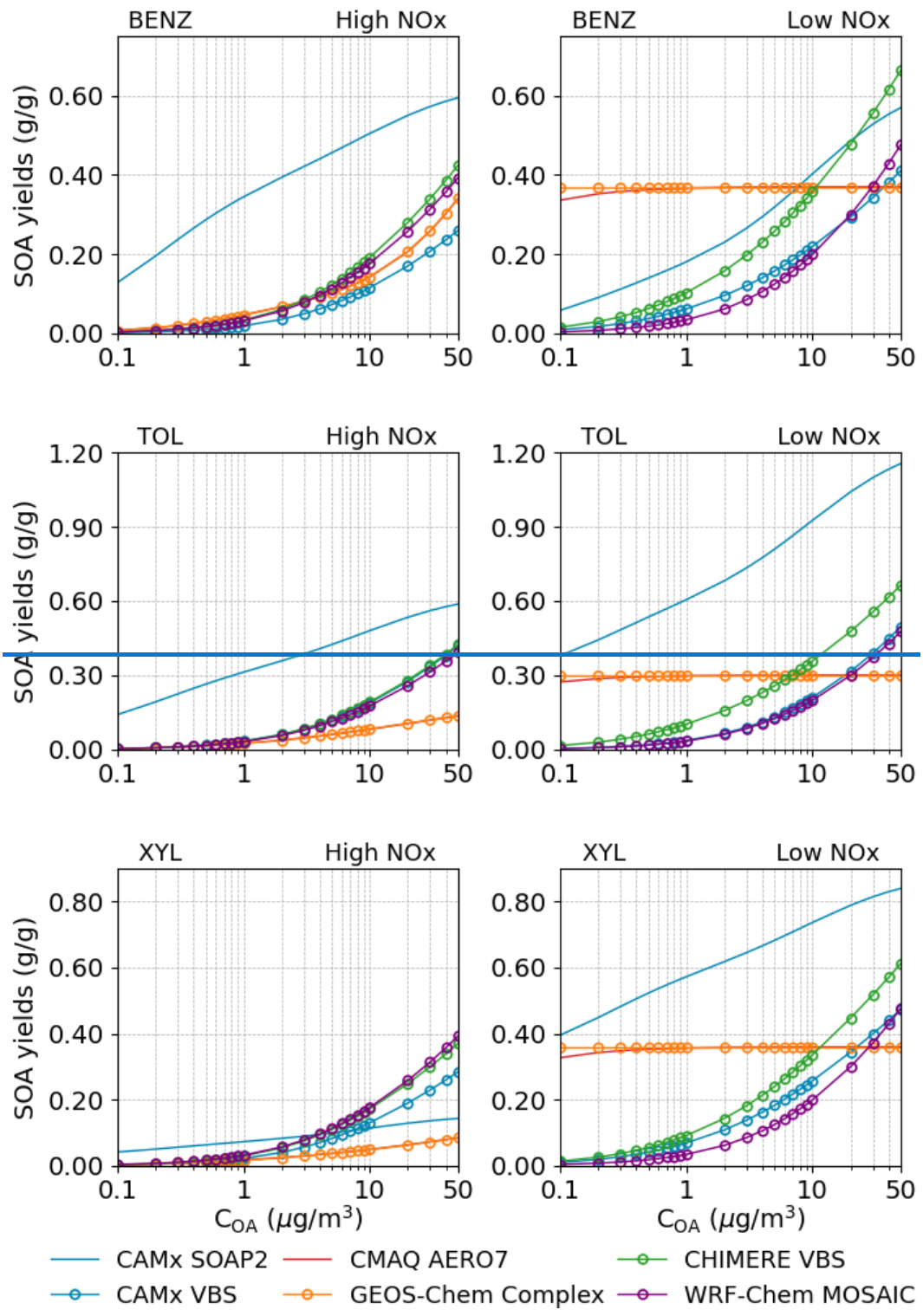
BENZ
High NOx
BENZ
Low NOx
TOL
High NOx
TOL
Low NOx
XYL
High NOx
XYL
Low NOx
SOA yields (g/g)
0.00
0.20
0.40
0.60
0.30
0.90
1.20
0.80
0.1
1
10
50
C_{OA} ($\mu g/m^3$)
CAMx SOAP2
CAMx VBS
CMAQ AERO7
GEOS-Chem Complex
CHIMERE VBS
WRF-Chem MOSAIC

438

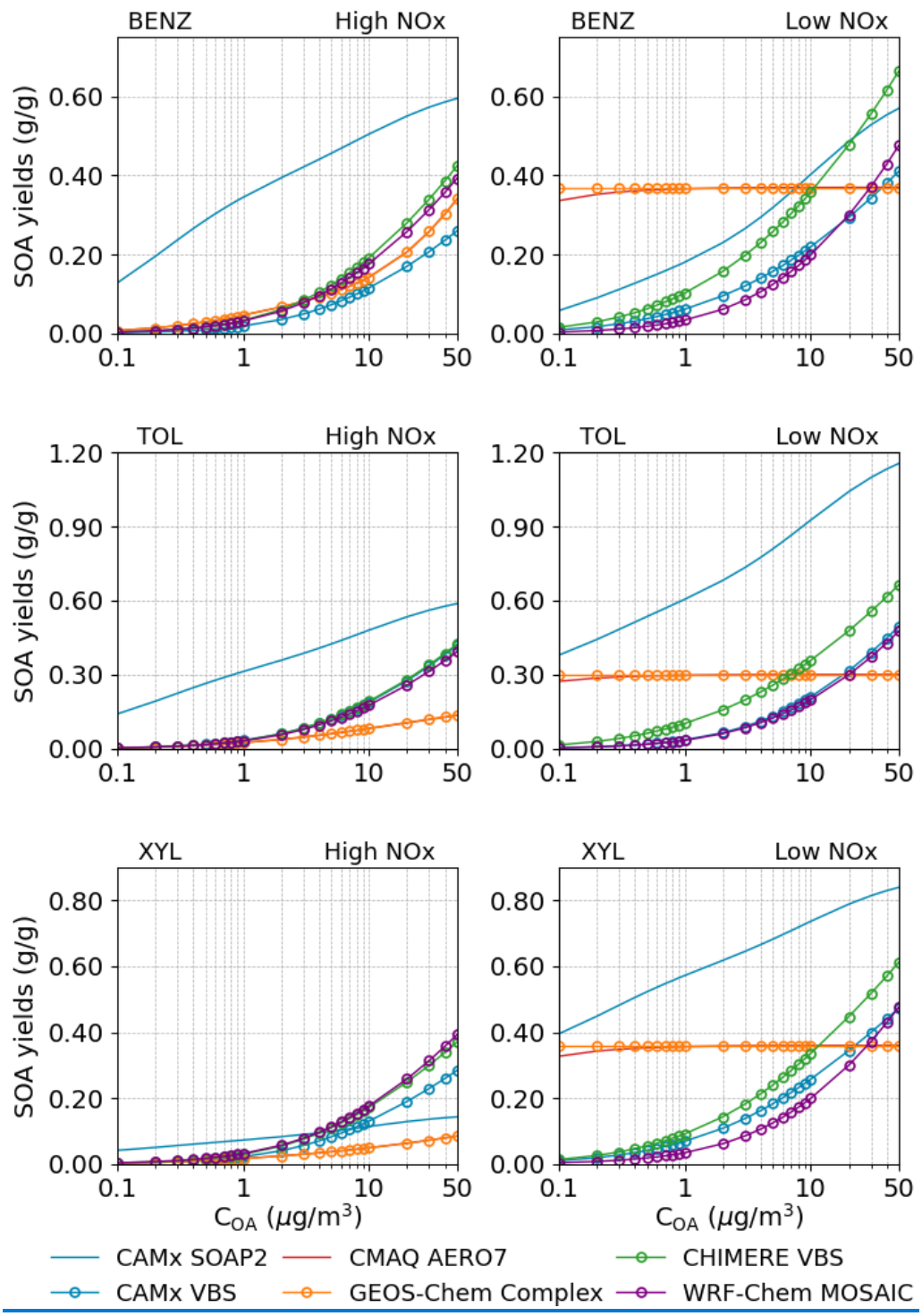

Figure 3 Comparison of the ~~initial~~non-aged SOA yields (g/g) as functions of C_{OA} for three anthropogenic VOC among different schemes (CMAQ CRACMM not included). SOA yields are calculated at 298 K. Note that y-axis scales vary by precursor to highlight scheme discrepancies across different yield magnitudes.

Table 2~~1 Initial~~ Non-aged SOA yields (g/g) for different precursors across schemes at 298 K and C_{OA} of 10 μg/m^3.

Precursor-NOx case	CMx[1] SP2	CMx VBS	CMQ AE7	CMQ CRM	G-C Spl	G-C Cpx	CMR VBS	W-C MOS	Avg[7]	Max/Min[8]
BENZ[2]-high	0.51	0.12	0.14	0	/	0.14	0.19	0.18	0.21	4.4
BENZ-low	0.40	0.22	0.37	0	/	0.37	0.36	0.20	0.32	2.0
TOL[3]-high	0.48	0.19	0.08	0	/	0.08	0.19	0.18	0.20	5.8
TOL-low	0.93	0.21	0.30	0	/	0.30	0.36	0.20	0.38	4.6
XYL[4]-high	0.11	0.13	0.05	0	/	0.05	0.17	0.18	0.12	3.6
XYL-low	0.74	0.26	0.36	0	/	0.36	0.34	0.20	0.38	3.7
IVOC[5] high	0.36	0.51	1.00	0	/	0.20	2.7×10^{-4}	2.7×10^{-4}	0.35	3715
IVOC-low	0.55	0.51	1.00	0	/	0.73	2.7×10^{-4}	2.7×10^{-4}	0.46	3715
ISOP-high	0.05	0.01	0.05	0	0.03	0.04	0.04	0.01	0.03	4.0
ISOP-low	0.09	0.03	0.05	0	0.03	0.04	0.07	0.02	0.05	3.8
TERP-high	0.14	0.09	0.17	0	0.10	0.09	0.13	0.10	0.12	1.8
TERP-low	0.21	0.18	0.17	0	0.10	0.19	0.25	0.18	0.18	2.5
SESQ[6]-high	0.52	0.22	0.44	0	0.10	0.84	0.20	0.22	0.36	8.4
SESQ-low	0.70	0.22	0.44	0	0.10	0.42	0.20	0.22	0.33	7.0

[1] Model name abbreviations are CMx for CAMx, CMQ for CMAQ, G-C for GEOS-Chem, CMR for CHIMERE, and W-C for WRF-Chem. Scheme name abbreviations are SP2 for SOAP2, AE7 for AERO7, Spl for Simple, Cpx for Complex, and MOS for MOSAIC.

[2] For WRF-Chem and CHIMERE, results for BENZ are based on ARO1.

[3] For WRF-Chem and CHIMERE, results for TOL are based on ARO1.

[4] For WRF-Chem and CHIMERE, results for XYL are based on ARO2. For CMAQ CRACMM, results for XYL are averages of XYE and XYM.

[5] For CMAQ CRACMM, IVOC yields are average of alkane and oxygenated IVOCs (see details in Table S1~~1~~7). For WRF-Chem MOSAIC, IVOC is assumed to have 50% oxygen.

[6] For CHIMERE, results for SESQ are based on humulene.

[7] Multi-model average yield excluding GEOS-Chem Simple for aromatics and IVOC, and excluding CRACMM for ISOP.

[8] Ratio of maximum to minimum yield.

43.1.2 ~~Initial~~Non-aged SOA yields from biogenic VOC

Figure 4~~Figure 4~~ shows how the ~~initial~~non-aged SOA mass yields depend on C_{OA} for three biogenic VOC (BVOC), namely isoprene (ISOP), monoterpenes (TERP), and sesquiterpenes (SESQ). For isoprene, CMAQ includes heterogeneous SOA formation from IEPOX (Pye et al., 2013), which is outside the scope of this evaluation and thus is not discussed in this study. Overall, the BSOA yield patterns closely resemble those of ASOA. All schemes, except for GEOS-Chem Simple, predict an increase in yields associated with C_{OA}. However, the magnitude of SOA yields varies significantly across schemes, ranging from 1.8 to 8.4 under high NO*x* conditions and 2.5 to 7.0 under low NO*x* conditions. Additionally, model predictions regarding the influence of NO*x* on BSOA yields are inconsistent, with some indicating an increase, others a decrease, and some showing no effect. For instance, SOA yields from ISOP under high NO*x* conditions, as simulated by two CAMx schemes, WRF-Chem MOSAIC, and CHIMERE VBS, are approximately half of those under low NO*x* conditions. In contrast, CMAQ AERO7 and GEOS-Chem schemes suggest that SOA yields are independent of NO*x* levels. Regarding TERP-derived SOA, all schemes, except for CMAQ AERO7 and GEOS-Chem Simple, predict more than 50% higher yields under low NO*x* conditions compared to high NO*x* conditions. The latter two schemes show no difference between NO*x* regimes. For SESQ, four models (CAMx VBS, CMAQ AERO7, CHIMERE VBS, and WRF-Chem MOSAIC) predict no distinction in SOA yields between high and low NO*x* conditions. Conversely, CAMx SOAP2 suggests higher yields under low NO*x* conditions, whereas the GEOS-Chem Complex scheme predicts the opposite.

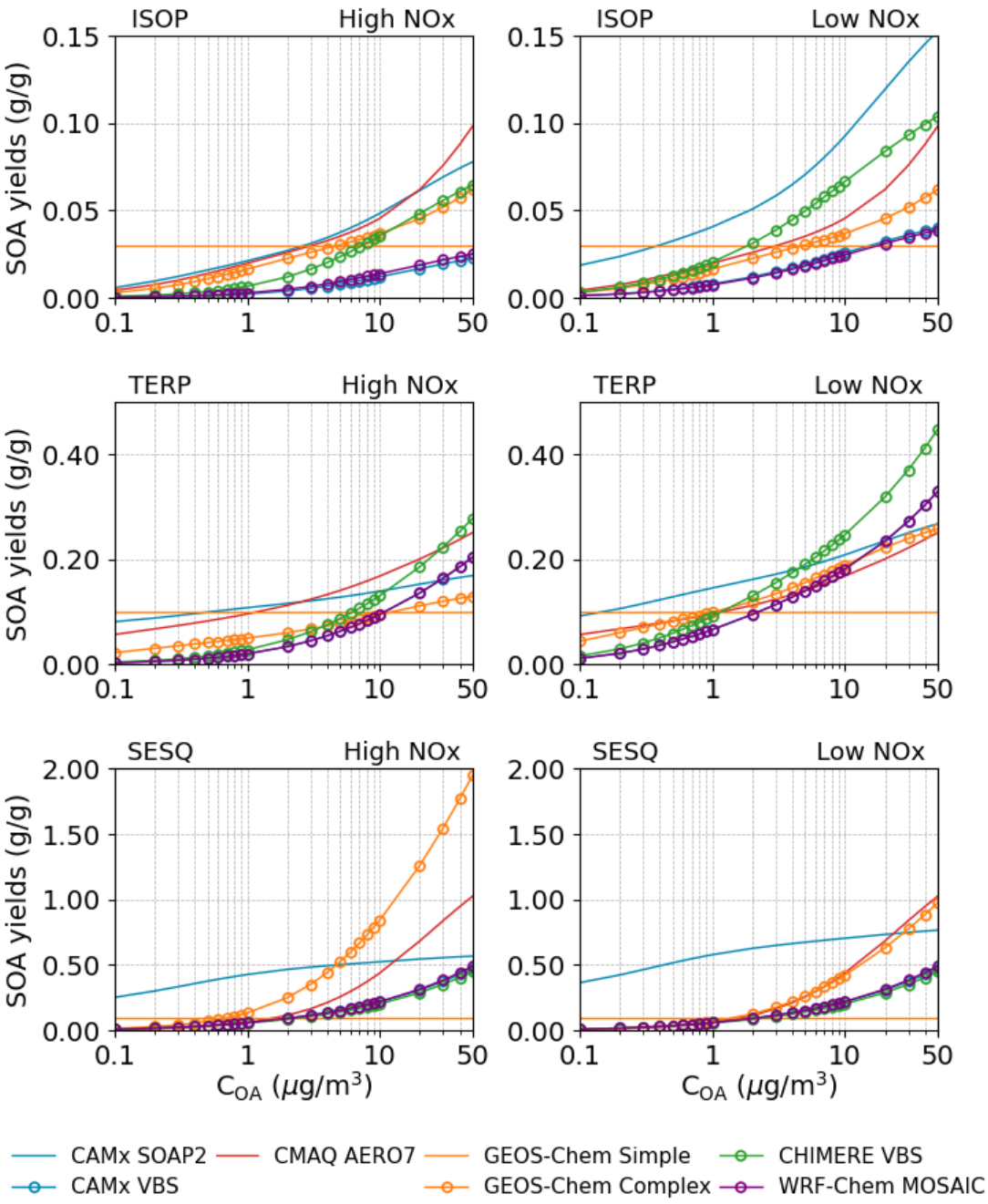

480

481 **Figure 4** Comparison of the ~~initial~~non-aged SOA yields (g/g) as functions of C_{OA} for three
482 biogenic VOC among different schemes (CMAQ CRACMM not included). SOA yields are
483 calculated at 298 K. Note that y-axis scales vary by precursor to highlight scheme
484 discrepancies across different yield magnitudes.

485 ~~4~~3.1.3 ~~Initial~~Non-aged SOA yields from intermediate volatility organic compounds (IVOC)

486 IVOC emissions make important contributions to ASOA formation (~~Robinson~~Zhao et al., 2016;
487 Ma et al., 2016; Zhao et al., 2014). The SOA yields from IVOC, referred to as IV-SOA,
488 predicted by each scheme are shown in Figure 5~~Figure 5~~. The GEOS-Chem Simple scheme is

omitted since it does not explicitly account for IVOC. Additionally, the results for CMAQ CRACMM are discussed separately in Section 4.2.3, due to its distinct treatment of several IVOC types.

SOA yields from IVOC in the CAMx VBS scheme shows a strong positive dependence on C_{OA} whereas CAMx SOAP2 and GEOS-Chem Complex exhibit much weaker responses. Constant SOA yields of 1.0 g/g are set in CMAQ AERO7, regardless of NO*x* levels, surpassing the values predicted by other schemes. SOA formation from IVOC in CHIMERE VBS and WRF-Chem MOSAIC is treated as multi-generational ~~oxidations (-),~~oxidation (R13-R18 in Supplementary Information), resulting in extremely low ~~initial~~non-aged SOA yields (<0.001 g/g).

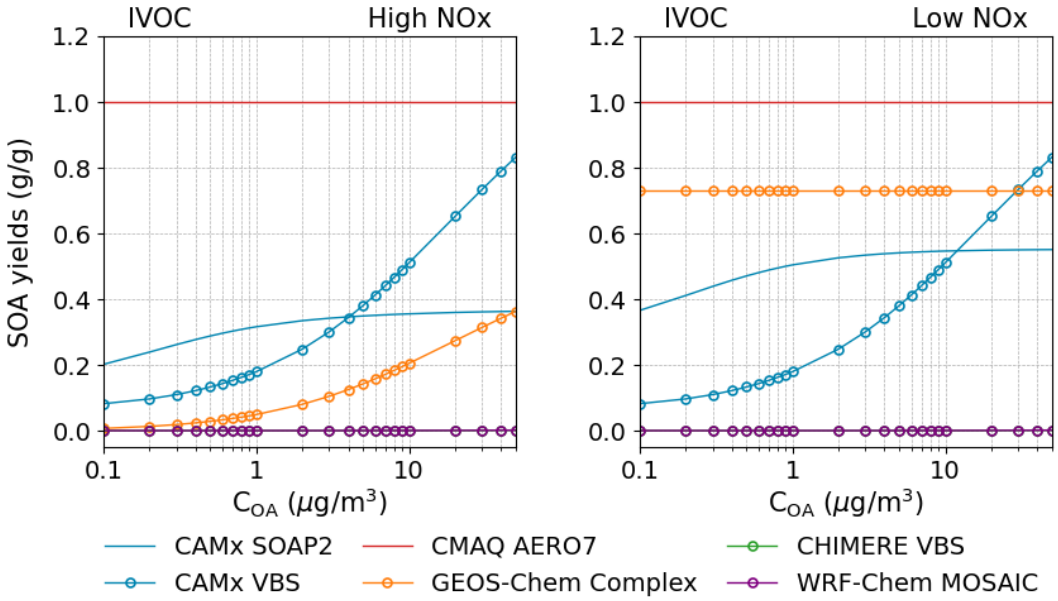

Figure 5 Comparison of the ~~initial~~non-aged SOA yields (g/g) as functions of C_{OA} for IVOC among different schemes (CMAQ CRACMM and GEOS-Chem Simple not included). SOA yields are calculated at 298 K.

43.2 Comparison of SOA aging

Among the eight schemes we evaluated, the CAMx SOAP2, GEOS-Chem Simple, and GEOS-Chem Complex schemes do not incorporate explicit SOA aging processes. However, the SOAP2 yields are derived from a VBS parameterization that includes aging (Hodzic et al., 2016) and may therefore be considered pre-aged (Emery et al., 2024). The remaining schemes account for SOA aging using one or more of three mechanisms: gas-phase OH-oxidation,

condensed-phase oligomerization, and condensed-phase hydrolysis. Gas-phase OH-oxidation aging is typically parameterized as functionalization reactions that generate less volatile products (e.g. Figure 2~~Figure 2~~b) and/or fragmentation reactions that produce more volatile products (e.g. Figure 2~~Figure 2~~c). This mechanism is adopted in CAMx VBS (for AVOC and IVOCs only), CMAQ CRACMM, WRF-Chem MOSAIC and CHIMERE VBS, with implementation being specific to each scheme. Condensed-phase oligomerization aging (e.g. Figure 2~~Figure 2~~d) is characterized as a first-order particle-phase reaction, usually assuming a lifetime of 30 hr, leading to non-volatile product formation independent of oxidant concentrations. CMAQ AERO7 applies this process for SOA formed from all precursors except monoterpenes. For SOA derived from NO_3 oxidation of monoterpenes, AERO7 instead applies condensed-phase hydrolysis, yielding non-volatile products with a lifetime of ~3 hr.

To compare the aging effects on SOA yields across different schemes, we assumed a 24-hour exposure to an OH concentration of 3×10^6 molecules/cm^3 (equivalent to 2.6×10^{11} molecules·s·cm^{-3}) for the OH-oxidation aging process or a 24-hour of condensed-phase oligomerization/hydrolysis when calculating the aged SOA yields (details presented below). Table 3~~Table 3~~~~Table 2~~ summarizes the aged SOA yields (when applicable) at 298 K with a C_{OA} of 10 µg/m^3 as simulated by each scheme. Figure 6~~Figure 6~~ and Figure 7~~Figure 7~~ further compare the ~~initial~~non-aged and aged SOA yields for each scheme and SOA precursor, while Figure 8~~Figure 8~~ separately illustrates the aging effects on IVOC-derived SOA across different schemes.

~~4~~3.2.1 Aging in CAMx VBS

The CAMx VBS scheme incorporates step-wise gas-phase OH-oxidation aging for AVOC and IVOC without accounting for fragmentation processes (Figure 2~~Figure 2~~b). The calculation of aged SOA yields follows Eq. 3~~Eq. 3~~ to Eq. 5~~Eq. 5~~, using a k_{OH} value of 2×10^{-11} cm^3 molecule^{-1} s^{-1} and an OH concentration of 3×10^6 molecules cm^{-3}. Figure 7~~Figure 7~~a-b illustrates how SOA yields change as a function of accumulated OH exposure under high and low NO*x* conditions for different precursors. In the CAMx VBS scheme, SOA yields increase with OH exposure though the rate of aging slows as the OH exposure increases. With a 24-hour period

(corresponding to an OH exposure of 2.6×10^{11} molecules·s·cm^{-3}), SOA yields from aromatics increase by a factor of 5-6 under high NO*x* conditions and 3-5 under low NO*x* conditions compared to their ~~initial~~non-aged yields. For IVOC, aged SOA yields increase by 125% relative to the ~~initial~~non-aged yields (Figure 8~~Figure 8(Figure 8bb~~). These findings highlight the significant influence of aging processes implemented in the CAMx VBS scheme.

Table 3~~2~~ Aged SOA yields (g/g) for different precursors across schemes at 298 K and C_{OA} of 10 µg/m^3. Shaded values indicate no aging effect (i.e. identical to values in Table 2~~Table 2Table 1).).~~

Precursor-NOx case	CMx[1] SP2	CMx VBS	CMQ AE7	CMQ CRM	G-C Spl	G-C Cpx	CMR VBS	W-C MOS	Avg[7]	Max/Min[8]
BENZ[2]-high	0.51	0.80	0.22	0.23	/	0.14	0.79	0.18	0.41	5.6
BENZ-low	0.40	1.07	0.37	0.67	/	0.37	1.11	0.20	0.60	5.6
TOL[3]-high	0.48	1.30	0.12	0.11	/	0.08	0.79	0.18	0.44	15.7
TOL-low	0.93	1.33	0.30	0.50	/	0.30	1.11	0.20	0.67	6.7
XYL[4]-high	0.11	0.83	0.07	0.09	/	0.05	0.66	0.18	0.29	16.9
XYL-low	0.74	1.14	0.36	0.51	/	0.36	0.98	0.20	0.61	5.7
IVOC[5] high	0.36	1.15	1.00	0.31	/	0.20	0.02	1.20	0.60	73.7
IVOC-low	0.55	1.15	1.00	0.53	/	0.73	0.02	1.20	0.74	73.7
ISOP-high	0.05	0.01	0.06	/	0.03	0.04	0.08	0.01	0.04	6.8
ISOP-low	0.09	0.03	0.06	/	0.03	0.04	0.12	0.02	0.06	5.0
TERP-high	0.14	0.09	0.17	0.84	0.10	0.09	0.54	0.10	0.26	5.7
TERP-low	0.21	0.18	0.17	0.20	0.10	0.19	0.80	0.18	0.25	17.5
SESQ[6]-high	0.52	0.22	0.78	0.54	0.10	0.84	0.86	0.22	0.51	8.6
SESQ-low	0.70	0.22	0.78	1.04	0.10	0.42	0.86	0.22	0.54	10.4

[1] Model name abbreviations are CMx for CAMx, CMQ for CMAQ, G-C for GEOS-Chem, CMR for CHIMERE, and W-C for WRF-Chem. Scheme name abbreviations are SP2 for SOAP2, AE7 for AERO7, Spl for Simple, Cpx for Complex, and MOS for MOSAIC.

[2] For WRF-Chem and CHIMERE, results for BENZ are based on ARO1.

[3] For WRF-Chem and CHIMERE, results for TOL are based on ARO1.

[4] For WRF-Chem and CHIMERE, results for XYL are based on ARO2. For CMAQ CRACMM, results for XYL are averages of XYE and XYM.

[5] For CMAQ CRACMM, IVOC yields are average of alkane and oxygenated IVOCs (see details in Table S1~~+~~7). For WRF-Chem MOSAIC, IVOC is assumed to have 50% oxygen.

[6] For CHIMERE, results for SESQ are based on humulene.

[7] Multi-model average yield excluding GEOS-Chem Simple for aromatics and IVOC, and excluding CRACMM for ISOP.

[8] Ratio of maximum to minimum yield.

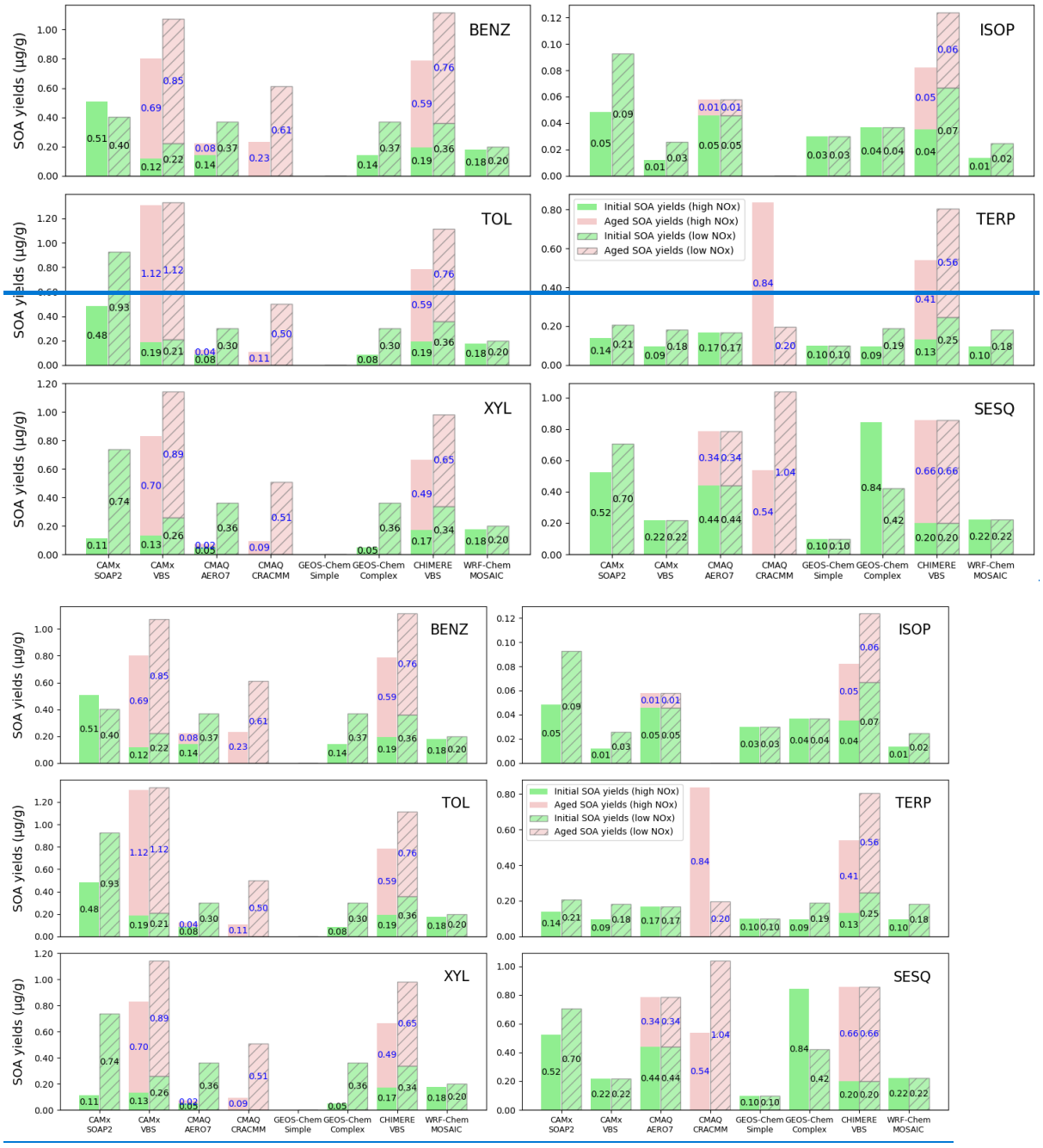

Figure 6 Effect of aging on SOA yields (g/g) for different precursors under high and low NO*x* conditions.

4 Note that y-axis scales vary by precursor to highlight scheme discrepancies across different yield magnitude.

3.2.2 Aging in CMAQ AERO7

The SOA aging process in the CMAQ AERO7 scheme involves particle-phase oligomerization (Figure 2~~Figure 2~~d) and hydrolysis. Oligomerization applies to SOA formed from ISOP, SESQ, and aromatics (only under high-NO*x* conditions) while hydrolysis affects SOA formed from monoterpenes oxidation by NO_3 radical. The aged SOA yields resulting from oligomerization and hydrolysis follows Eq. 6~~Eq. 6~~ to Eq. 8~~Eq. 8~~, with rate constants $k_{OLIG} = 9.49\times10^{-6}\ s^{-1}$ and $k_{hydro} = 9.26\times10^{-5}\ s^{-1}$. Figure 7~~Figure 7~~b illustrates the evolution of SOA yields over 24 hours of oligomerization, showing increases of 27%, 79%, and 46%-57% for ISOP, SESQ, and aromatics, respectively. This increase results from the reduced volatility of SOA due to oligomerization. The hydrolysis reaction, assuming a shorter lifetime of approximately 3 hr, leads to a 48% increase in SOA yield from monoterpene-derived organic nitrates over 1 day. Although the hydrolysis rate is nearly ten times faster than that of oligomerization, the overall yield increase is moderated because the hydrolysis products have lower molecular weights than their parent compounds.

43.2.3 Aging in CMAQ CRACMM

The aging processes in CMAQ CRACMM involve the gas-phase OH-oxidation reactions of secondary oxygenated L/S/IVOCs, leading to both fragmentation and functionalization, and resulting in products with varying volatilities. As illustrated in Figure 7~~Figure 7~~e-f, the impact of aging on SOA yields depends on the precursor and varies between high NO*x* and low NO*x* conditions. Under high NO*x* conditions, SOA yields from all precursors increase substantially during the first 6-8 hours, after which the growth rate becomes negligible (except for TERP, which continues to increase). After 24 hours of aging, SOA yields under high NO*x* conditions range from 0.093 g/g for XYL to 0.838 g/g for TERP (Table 3~~Table 3~~~~(Table 2).~~). In contrast, under low NO*x* conditions, all precursors show a sharp increase in SOA yields within the first 30 mins. Subsequently, SOA yields from XYL begin to decline, gradually reaching a minimum

value of approximately 0.511 g/g after 16 hours. On the contrary, BENZ yields continue to increase slightly, peaking around 0.670 g/g. TERP, TOL, and SESQ yields exhibit minimal change after their initial increase. After 24 hours, SOA yields under low NO*x* conditions range from 0.195 g/g for TERP to 1.039 g/g for SESQ.

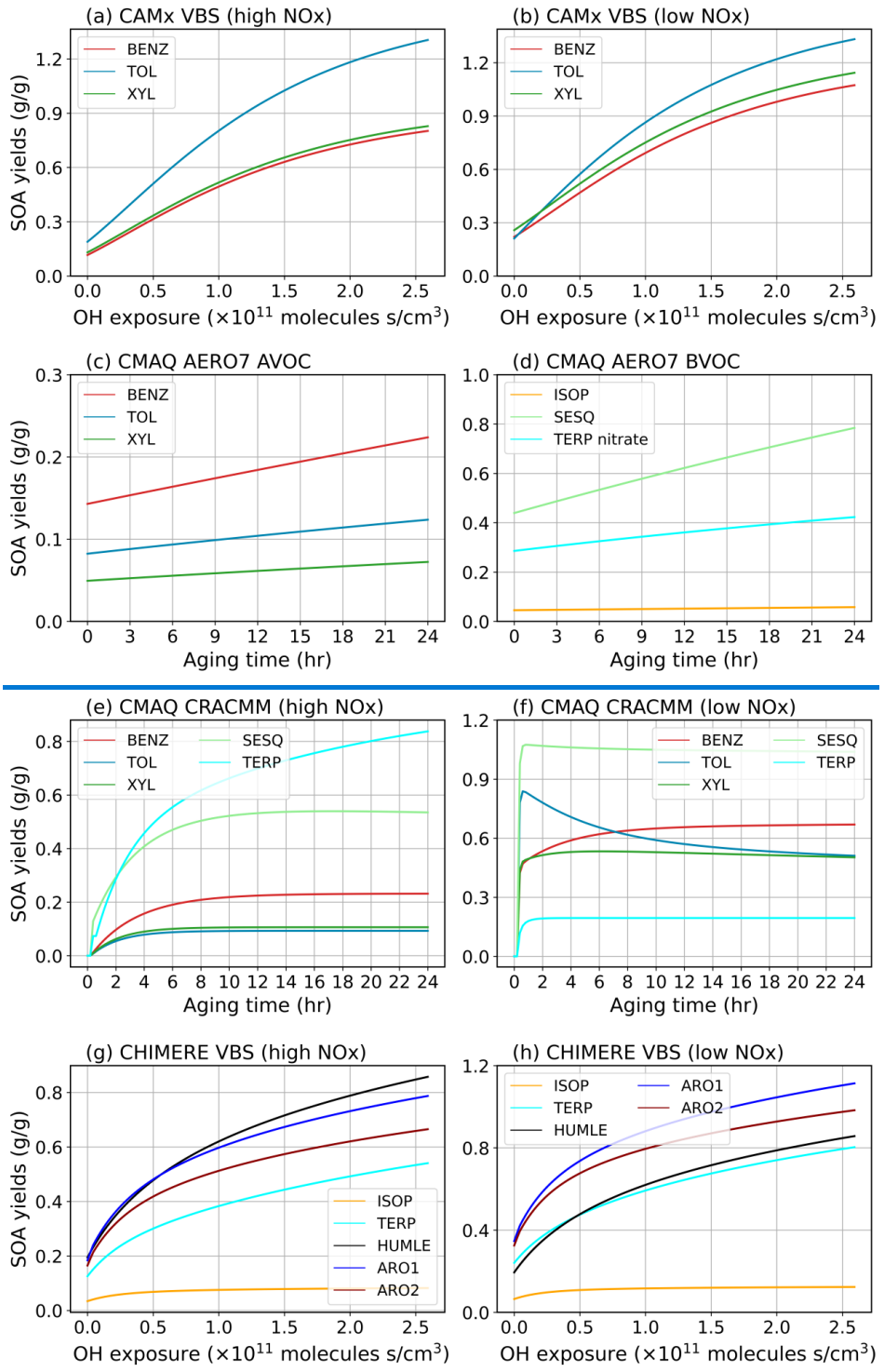

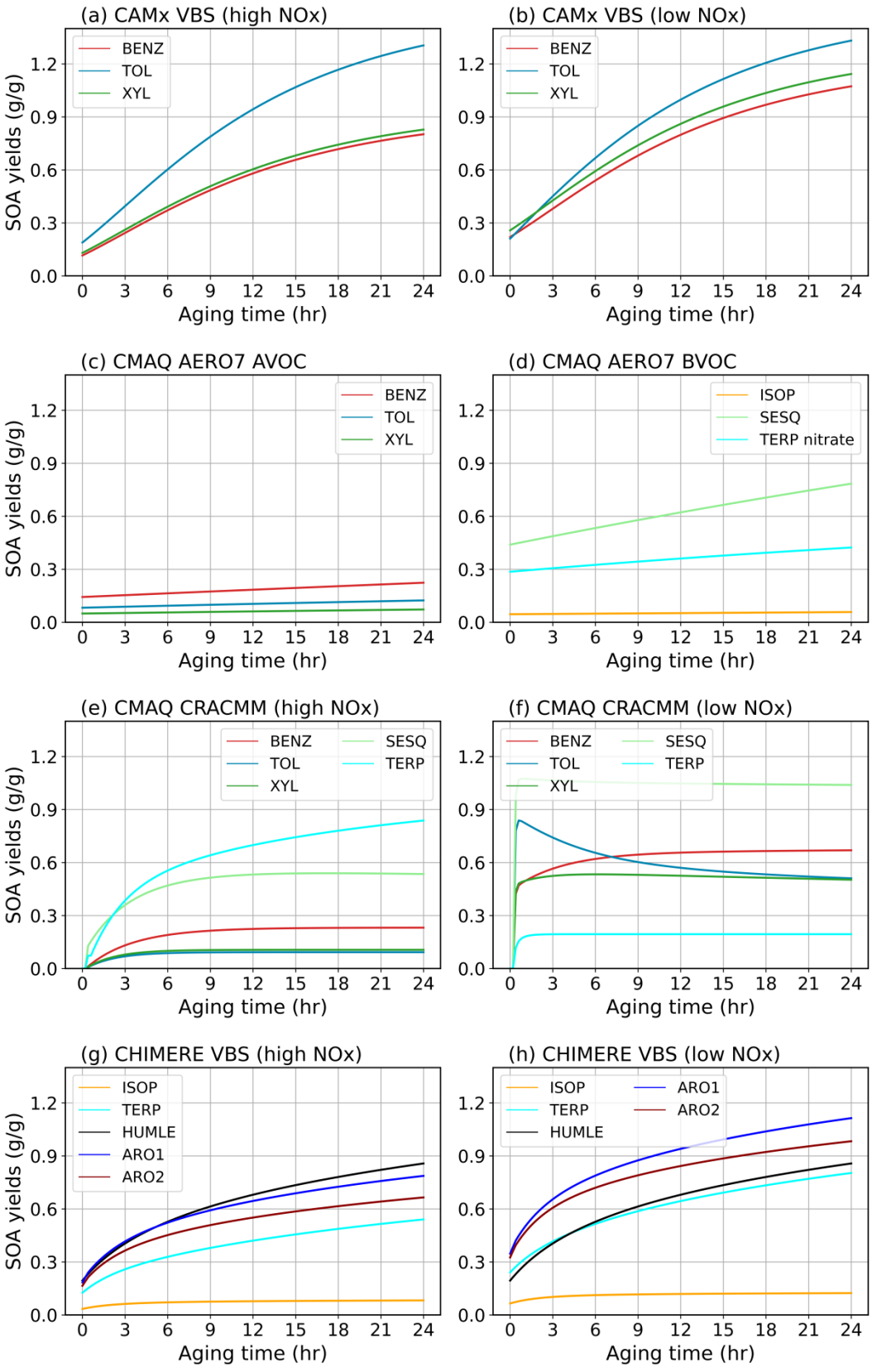

Figure 7 Effect of aging on SOA yields (g/g) from different precursors as a function of OH exposure or aging time in different schemes. (a-b) CAMx VBS; (c-d) CMAQ

AERO7; (e-f) CMAQ CRACMM; and (g-h) CHIMERE VBS. The numbers in the brackets indicate the relative change of SOA yields at hour 24 to hour 0.

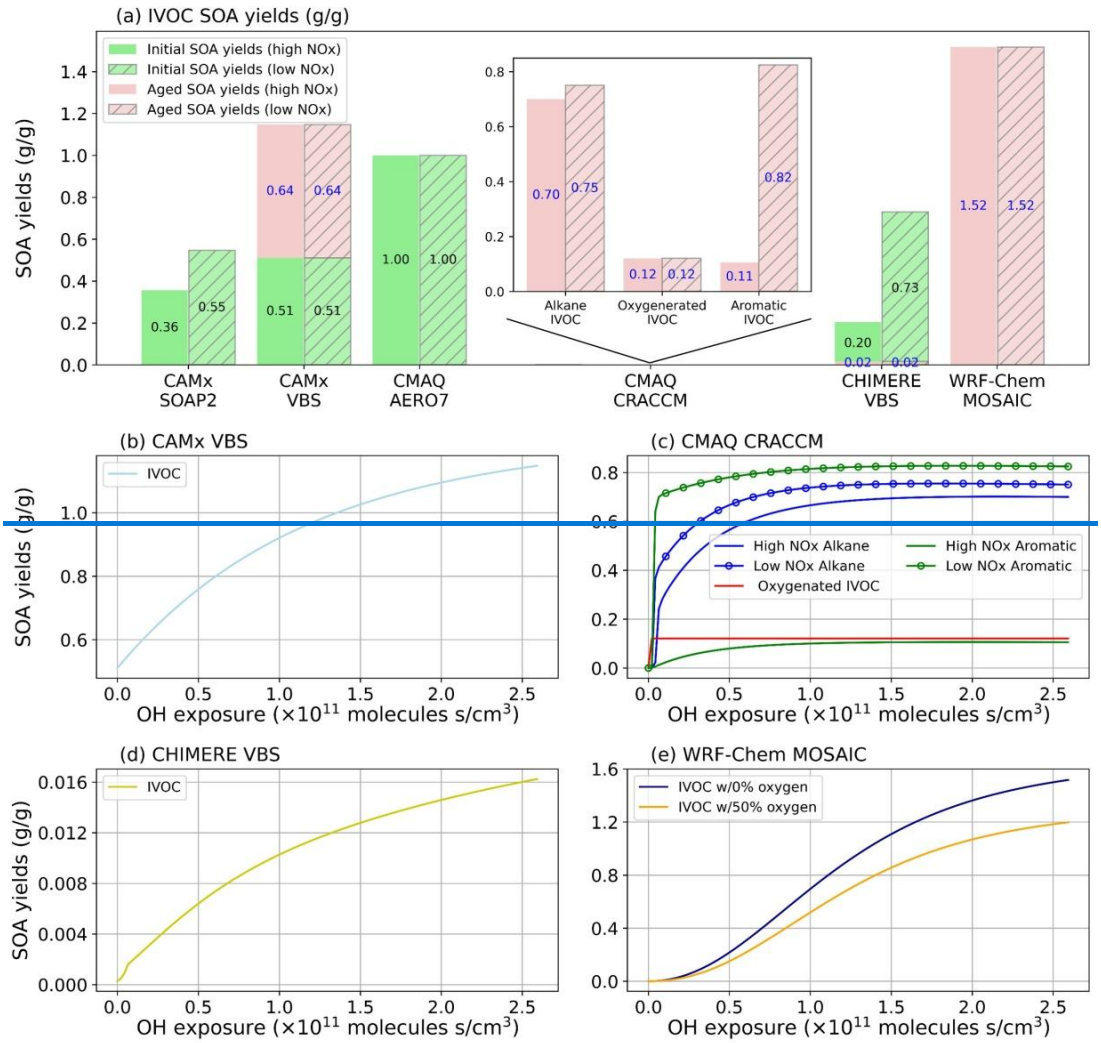

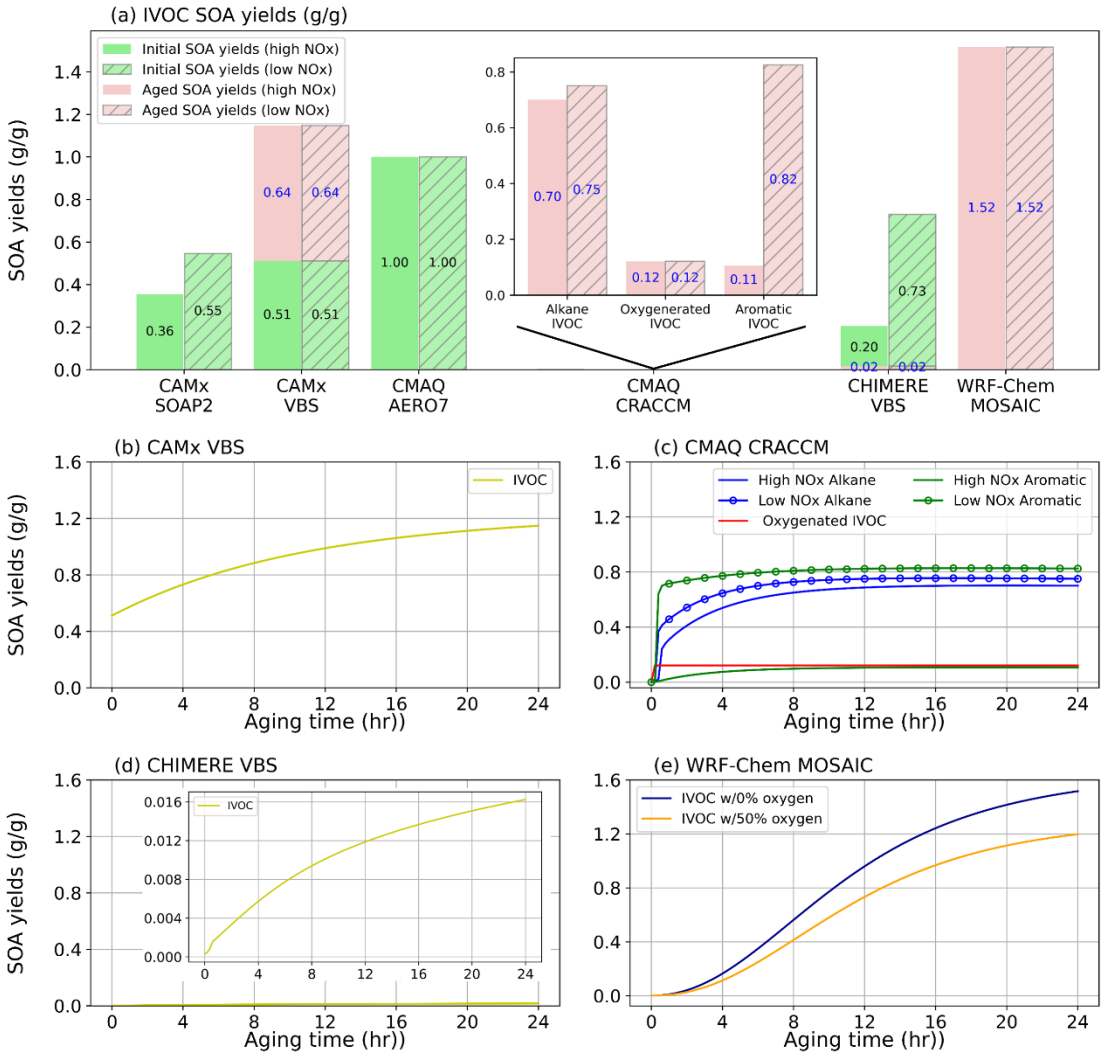

Figure 8 Effect of aging on SOA yields (g/g) for IVOC precursors under high and low NO*x* conditions for different schemes.

Unlike other schemes, the CMAQ CRACMM scheme classifies IVOC into alkanes, aromatics, and oxygenated IVOC based on their functional groups. Emitted oxygenated IVOC do not exhibit aging effects, as their oxidation products are assumed to be non-volatile (Figure 8~~Figure 8~~(~~Figure 8ec~~). In contrast, SOA yields from alkane and aromatic IVOC increase with the aging time, with the growth rate becoming negligible after approximately 10 hours. SOA yields from oxygenated IVOC (0.121 g/g) are independent of NO*x* conditions. The other two IVOC types show higher SOA yields under low NO*x* conditions, particularly for aromatic IVOC, where the SOA yields under low NOx conditions (0.825 g/g) are nearly 8 times that under high NO*x* conditions (0.105 g/g).

43.2.4 Aging in CHIMERE VBS

The CHIMERE VBS scheme accounts for aging through gas-phase functionalization and fragmentation, as well as condensed-phase oligomerization, as shown in Supplementary Information R9 to ~~.~~R12. Figure 7~~Figure 7~~d presents the combined aging effects on SOA over a 24-hour period under this scheme. Among BVOC, the aging effect is more pronounced for TERP and humulenes (HUMULE) than for ISOP. Under high NO*x* conditions, the SOA yields from ISOP, TERP, and HUMULE increase by 141%, 331%, and 341%, respectively, over one day. In contrast, under low NO*x* conditions, the aging effect is generally less significant, except for HUMULE, which exhibits a similar level of aging under both NO*x* regimes. Aromatics show substantial increase in SOA yields—over 300% under high NO*x* and 200% under low NO*x* conditions.

Aging of SOA from IVOC results in a dramatic increase in yields—by nearly a factor of 60 within one day, as shown by Figure 8~~Figure 8~~d. However, the absolute SOA yields from IVOC remain low (approximately 0.01 g/g), which is attributed to the ~~initial~~non-aged low SOA formation (~10^{-4} g/g) and the dominance of fragmentation at higher oxidation generations. From the third oxidation generation onward, 75% of the condensable gases undergo fragmentation into more volatile products, while only 15% undergo functionalization, as described in ~~.~~Supplementary Information R14.

43.2.5 Aging in WRF-Chem MOSAIC

The WRF-Chem MOSAIC scheme does not include SOA aging processes for AVOC and BVOC. SOA formation from IVOC is parameterized as a stepwise gas-phase OH-oxidation process. For the non-oxygen component of condensable gases, a 15% mass gain is assumed for each generation (as per Supplementary Information R15 and ~~).~~R16). Meanwhile, the oxygenated component shifts to lower volatility bins without mass gain (as per Supplementary Information R17 and ~~).~~R18). The scheme does not consider fragmentation or condensed-phase oligomerization. Figure 8~~Figure 8~~e illustrates aging effects under two scenarios: IVOC with hydrocarbon-like characteristics (0% oxygen by mass at t=0, representing of diesel emissions) and IVOC with 50% oxygen by mass

(representing of biomass burning emissions). In both cases, the non-fragmenting stepwise aging process in WRF-Chem results in substantial increases in SOA yields. At an OH exposure of 2.6×10^{11} molecule·s·cm^{-3} (i.e. a 24-hour period), SOA formed from hydrocarbon-like IVOC exceeds 1 g/g, despite an initially negligible yield.

43.3 NO*x* effects on SOA yields

Evaluating SOA yields for seven precursor types across eight modeling schemes results in 56 potential characterizations of how NO*x* levels influence SOA formation. Table S128 and S139 present the ratios of ~~initial~~non-aged and aged SOA yields under high and low NO*x* conditions. For ~~initial~~non-aged SOA yields, 11 of the 56 cases are missing and 14 cases are designed to exhibit no NO*x* dependence, leaving 31 meaningful comparisons. Among these, 29 cases show lower SOA yields under high NO*x* conditions. For aged SOA yields, 5 cases are missing and 14 are designed with no NO*x* effect, leaving 37 meaningful comparisons, of which 34 also show lower SOA yields under high NO*x* conditions. These results indicate a general trend of higher SOA yields under low NO*x* conditions, although a few exceptions are observed. In some cases, the NO*x* effect is reversed—that is, SOA yields are higher under high NO*x* conditions than under low NO*x* conditions. This is seen for BENZ in the CAMx SOAP2 scheme, TERP in CMAQ CRACMM, and SESQ in the GEOS-Chem Complex scheme. The NO*x* effect on terpene-derived SOA in CRACMM is particularly noteworthy: the model predicts an eightfold increase in SOA yields under high NO*x* conditions compared to low NO*x*. This is significant given that terpenes are key SOA precursors in many forested regions, such as the Eastern U.S., where anthropogenic NO*x* emissions may change due to ongoing urban development (which could increase NO*x* levels) or the implementation of emission control technologies (which may reduce them). Experimental studies, including those by Sarrafzadeh et al. (2016) and Wildt et al. (2014), have consistently found that terpene-derived SOA yields are higher under low NO*x* conditions, a result that aligns with most of the evaluated schemes but contrasts with the predictions made by CRACMM.

3.4 SOA variations in box model simulations

The box model simulations reveal significant discrepancies in predicted SOA concentration and composition among the selected schemes at both the urban (DFW) and rural (TYL) locations (Figure 9). The total SOA concentrations can vary by a factor of 2–3 between schemes even under identical meteorological and emission inputs. Overall, SOA concentrations are higher at DFW than at TYL. At both locations, all schemes exhibit a consistent diurnal profile characterized by SOA accumulation throughout the day and night, followed by a sharp decline in the early morning (beginning around 06:00 LST) caused by expansion of the planetary boundary layer (PBL). At DFW, the temporal trends are similar across the four schemes; however, the magnitude varies, with Simple and AERO7 predicting the highest concentrations, while CRACMM predicts the lowest. At TYL, the inter-model spread is narrower than at DFW. Notable differences in diurnal dominance emerge: SOAP2 and CRACMM predict the highest concentrations overnight—a pattern distinct from DFW—while Simple and CRACMM produce the highest values during daytime hours. Figure 9~~Figure 9~~c-d shows the maximum and minimum average SOA concentrations. At DFW, Simple and CRACMM predict the highest and lowest total SOA concentrations, respectively. Conversely, at TYL, CRACMM predicts the highest average concentration, while AERO7 predicts the lowest.

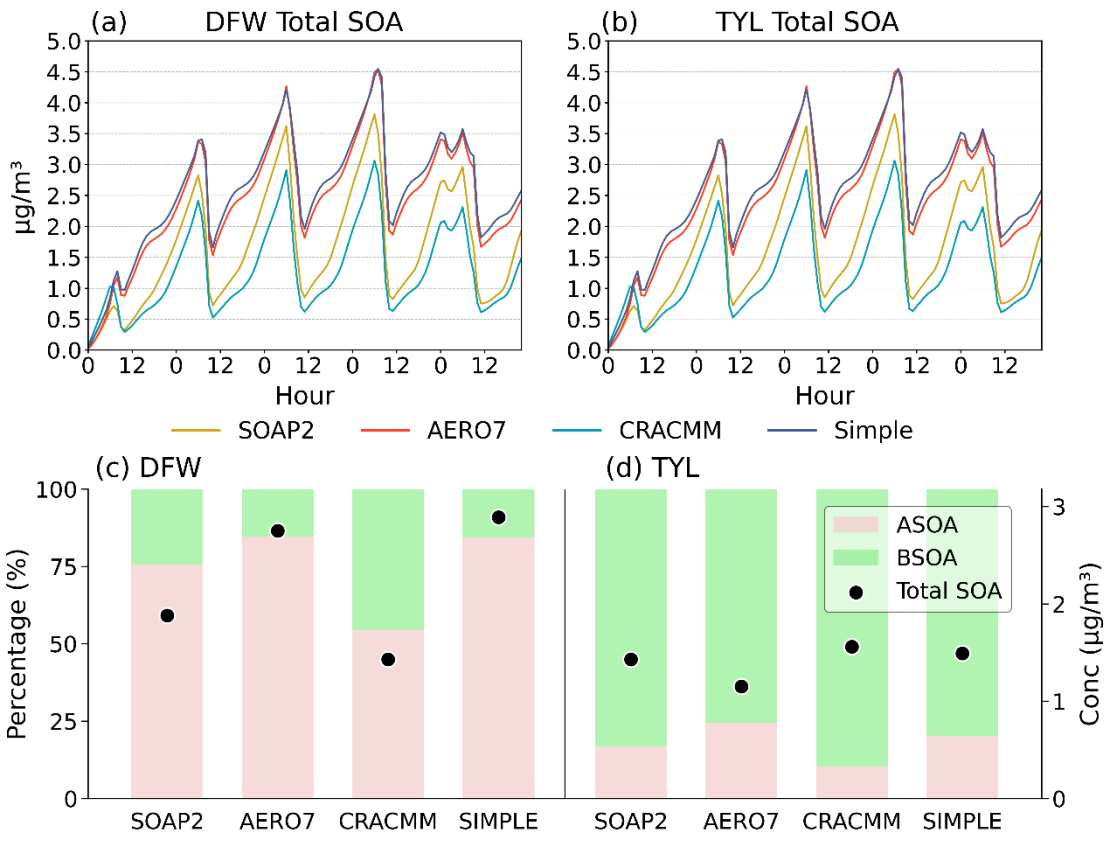

Figure 9 Diurnal profiles of total SOA (µg/m^3) from the 5-day box model base simulations at (a) DFW and (b) TYL. Average SOA concentrations (µg/m^3) averaged over days 2 through 5 of base model simulations for each SOA scheme (circles) and average contributions of ASOA and BSOA (bars)

Response surface plots for 24-hour average SOA concentrations derived from the matrix of simulations with varied anthropogenic NO*x* and VOC emissions are presented in Figure S4-S5. At DFW, total SOA concentrations generally decrease as anthropogenic NO*x* emissions increase relative to the base case (scaling factors 2–9) for all schemes, with the notable exception of CRACMM. CRACMM predicts negligible changes or a slight increase in SOA as NO*x* rises from low to mid scaling factors and a decrease is observed only when NO*x* emissions are increased by about a factor of 7 or greater. CRACMM also predicts the lowest SOA concentrations across all scaling factors. AERO7 and SIMPLE are very similar in both response surface shape and magnitude. For each scheme, SOA concentrations decrease as the anthropogenic VOC emissions decrease. At TYL, the response surfaces for AERO7, Simple, and SOAP3 are similar, with SOA concentrations remaining relatively constant at NO*x*

scaling factors greater than 1. In contrast, CRACMM demonstrates a much stronger response, with SOA mass increasing concurrently with NO*x* emissions. At this biogenic-dominated site, SOA concentrations in all schemes are minimally sensitive to variations in anthropogenic VOC emissions.

Understanding how SOA responds to NO*x* reductions is critical for near-term air quality planning, as many regulatory strategies (e.g., cleaner vehicles, energy transition) produce substantial NO*x* emissions abatement (Crippa et al. 2016; EPA et al. 2017; Li et al. 2024). Table 4~~Table 4~~ summarizes the impact of a 50% reduction in NO*x* emissions on total SOA, ASOA, and BSOA. In all schemes, reducing NO*x* leads to increased ASOA concentrations, with the most pronounced increase predicted by SOAP2. SIMPLE predicts the smallest increase in ASOA at DFW, while CRACMM predicts the smallest increase at TYL. At DFW, this NO*x* reduction also drives an increase in BSOA concentrations across most schemes, with the notable exception of CRACMM. Consistent with the ASOA results, SOAP2 predicts the largest increase in BSOA. The distinct behavior in CRACMM is driven by its monoterpene SOA parameterization; contrary to other schemes and experimental evidence (Lane et al. 2008; Sarrafzadeh et al. 2016, Zhao et al. 2018), CRACMM predicts decreasing yields under lower NO*x* conditions. Consequently, the substantial reduction in BSOA predicted by CRACMM at DFW results in a net decrease in total SOA, a trend opposite to that observed in the other schemes. At TYL, all schemes predict a decrease in both BSOA and total SOA, with the most significant reductions observed in the CRACMM simulation. The dominance of biogenic emissions at TYL compared to DFW is reflected in the significantly higher BSOA concentrations. The differing SOA responses to NO*x* reduction between the two sites are attributable to the distinct biogenic emission regimes producing different VOC/NO*x* emission ratios.

Table 4 Average concentrations (μg/m^3) of anthropogenic SOA (ASOA) and biogenic SOA (BSOA) over days 2 through 5 for the base and reduced NOx model simulations. Shading indicates a decrease in SOA concentrations in the reduced NO*x* model runs compared to the base runs.

Location	Species	SOAP2			AERO7		
		Base	50% NO*x*	Diff (%)	Base	50% NO*x*	Diff (%)
DFW	ASOA	1.34	1.48	9.60%	2.34	2.38	1.90%
	BSOA	0.42	0.48	12.20%	0.41	0.42	0.40%
	Total SOA	1.76	1.96	10.30%	2.75	2.8	1.60%
TYL	ASOA	0.24	0.25	4.40%	0.28	0.31	9.90%
	BSOA	1.19	1.14	-4.10%	0.87	0.82	-6.20%
	Total SOA	1.43	1.4	-2.50%	1.16	1.14	-1.80%
Location	Species	CRACMM			Simple		
		Base	50% NO*x*	Diff (%)	Base	50% NO*x*	Diff (%)
DFW	ASOA	0.78	0.81	3.50%	2.44	2.45	0.60%
	BSOA	0.65	0.59	-10.70%	0.45	0.46	2.40%
	Total SOA	1.43	1.4	-2.50%	2.88	2.91	0.90%
TYL	ASOA	0.16	0.17	1.00%	0.3	0.32	8.50%
	BSOA	1.4	1.24	-12.60%	1.19	1.14	-4.40%
	Total SOA	1.56	1.41	-11.00%	1.49	1.46	-1.50%

4. Implications

SOA schemes implemented in CTMs are diverse, making quantitative comparisons inherently challenging. CTMs employ diverse approaches to simulate SOA, from simple schemes that treat SOApre as non-volatile to more complex VBS schemes that utilize multiple basis sets to represent different types of precursors. Variability in how SOA aging is treated further adds to the overall diversity across schemes. In our view, such diversity is valuable from a research perspective, given that the underlying processes driving SOA formation remain uncertain and, in many cases, poorly characterized. The variation in SOA yields across different schemes reflects the extent of these uncertainties. The differences in scheme formulation, coupled with the large numbers of parameters employed in some schemes, pose practical challenges for applying multiple schemes to standardized scenarios. Addressing these challenges may require innovative approaches. Nonetheless, comparisons under standardized

conditions are essential for achieving meaningful quantitative inter-comparisons. Evaluating SOA yields under standard conditions and plotting SOA yield curves (i.e., yield vs. C_{OA}) are effective strategies for identifying similarities and differences among schemes. However, it is important to note that the results presented here may not fully capture the ranges of conditions encountered in three-dimensional atmospheric simulations.

~~Initial~~Non-aged SOA yields vary substantially across schemes and while many schemes consider SOA aging, the aging effects vary. Evaluating seven precursor types under both high and low NO*x* conditions yields 14 distinct comparisons. Across these comparisons, the ratio of maximum to minimum ~~initial~~non-aged yields (max/min) ranges from 1.8 to >1000 with a median max/min of 4.2 (Table 2~~Table 2(Table 1).~~). Among the eight schemes examined, three (CAMx SOAP2, GEOS-Chem schemes) do not include explicit SOA aging processes. Four schemes account for aging in a subset of precursor types and/or NO*x*-conditions, while only one (CMAQ CRACMM) includes aging for all precursors. Aging mechanisms considered by these schemes include gas-phase OH-oxidation of evaporated SOA, particle-phase oligomerization, hydrolysis, and photolysis. The impacts of aging on SOA yields vary by scheme and precursor (Table ~~S14~~S20): in 67 of the 98 evaluated cases (defined as one scheme/precursor/NO*x*-condition combination, CRACMM excluded), aging has no effect; in 31 cases, it increases SOA yields. Considering the aging effects, the ratio of max/min aged yields ranges from 5.0 to > 70, with a median value of 8.3 (Table 3~~Table 3(Table 2).~~). The relative rankings of precursors by their initial/aged SOA yields differ across schemes (Table S21~~5~~ and Table ~~S16~~S22), indicating that different aging schemes can lead to divergent conclusions regarding the relative importance of specific SOA precursors—a consideration with potential implications for policy guidance. For instance, discrepancies in yields lead to different precursor rankings (e.g., the relative importance of aromatics vs. IVOCs). A model that underpredicts the SOA potential of

IVOC emissions might disproportionately focus policy strategies on traditional VOCs (e.g., from petroleum-based solvents) and potentially lead to ineffective widespread controls that miss the critical contribution of IVOCs.

SOA aging remains an area in need of improved representation, with careful attention required to ensure consistent underlying assumptions. Notably, only the two CAMx schemes incorporate condensed-phase SOA photolysis, despite growing evidence that both anthropogenic and biogenic SOA can undergo substantial photolytic depletion (Hodzic et al., 2016; Baboomian et al., 2020), although a portion of SOA appears recalcitrant to such degradation (O'Brien and Kroll, 2019).

Large uncertainty exists for IVOC SOA yields. The SOA yields from IVOCs show wider variation (from negligible to 1.0 g/g) than for other anthropogenic precursors ~~(Table 1~~(Table 2~~Table 2~~ and Table 3~~Table 3~~~~Table 2),~~), partly due to different assumptions across schemes. For example, schemes such as WRF-Chem MOSAIC and CHIMERE VBS predict very low ~~initial~~non-aged yields from IVOC, based on the assumption that several generations of oxidation are required before forming condensable products. Even after one day of aging, IVOC SOA yields remain highly variable, ranging from 0.02 to 1.20 g/g. Although IVOC are generally classified based on volatility, factors such as high molecular weight or the presence of polar functional groups can shift compounds into the IVOC volatility range (Pankow and Asher, 2008). As a result, volatility and SOA yield are not necessarily well correlated (Donahue et al., 2011). Improving model representations of IVOC-derived SOA yields will require more detailed differentiation of IVOC emissions into multiple subtypes, as illustrated by the CRACMM scheme (Pye et al. 2023). A unified classification or "lumping" scheme for IVOC would be particularly advantageous, allowing multiple models to utilize a common emissions framework and enabling more direct comparisons of IVOC SOA yields. Improving the representation of oxygenated VOCs with reduced volatility—such as glycols and glycol ethers—within gas-phase chemical mechanisms can also

support improved differentiation of IVOC-related SOA formation (Yarwood and Tuite, 2024; Yu et al., 2024). More generally, a yield-based lumping approach for IVOCs (e.g., categorizing them into low, medium, or high yield classes) may be more practical to implement than strictly chemically-based schemes.

Determining experimental SOA yields also presents significant challenges. Laboratory experiments play a crucial role in guiding SOA model development and constraining key model parameters, particularly yields. However, these experiments are subject to operational and design limitations, including the need to account for chamber wall effects (Zhang et al., 2014) and to achieve atmospherically relevant concentration ranges (Peng et al., 2022; Kenagy et al., 2024). The role of autoxidation reactions in SOA formation further complicates the design of atmospherically relevant experiments, as discussed in detail by Kenagy et al. (2024). For instance, studying a reaction mechanism that includes RO_2 radical autoxidation at a rate of 0.1 s^{-1} requires that the effective rates of competing bimolecular reactions, particularly RO_2 + NO, be reduced to 0.1 s^{-1} or lower. This necessitates NO mixing ratios below approximately 5 ppb, which are now typical of photochemically active urban environments such as Los Angeles (Praske et al., 2018). Many SOA chamber experiments designed to investigate high NO*x* conditions exceed 5 ppb NO, thereby preventing autoxidation. Some chamber experiments, such as those by Sarrafzadeh et al. (2016), have been specifically designed to achieve atmospherically relevant NO (and other radicals) concentrations, making their results particularly valuable for SOA model development. In contrast, oxidation flow reactors face greater challenges (Peng et al., 2019) than chamber experiments in studying SOA formation due to their amplification of radical concentrations, which significantly shortens RO_2 lifetime and effectively suppresses autoxidation reactions. Wennberg (2023) has suggested shifting from the conventional terminology of high/low NO*x* to high/low NO to emphasize the critical role of NO concentration in determining RO_2 radical fate.

5. Conclusions

In this study, we compared SOA formation by eight schemes implemented in five widely used CTMs. For each SOA scheme, we quantified the ~~initial~~non-aged SOA mass yields under standardized conditions (T=298 K and C_{OA}=10 µg/m^3), showed how the ~~initial~~non-aged yield varies with C_{OA}, and quantified how one day of simulated atmospheric aging changed the ~~initial~~non-aged yield. We calculated yields for 7 SOA precursor types (4 anthropogenic and 3 biogenic) under both high and low NO*x* conditions.

The lack of consistency across eight current SOA schemes reviewed here reveals a lack of consensus within the air quality modelling community, notwithstanding substantial efforts to greatly expand the scientific knowledge base related to SOA formation over recent decades. Evaluating SOA schemes using ambient measurements is unlikely to produce consensus because large uncertainties in the SOA schemes are confounded with large uncertainties in precursor emission estimates. In our view, there is no objective basis for preferring one SOA scheme over another considering the high degree of uncertainty presented here. Complex SOA schemes may be valuable to research for investigating linkages between precursors and SOA, but conversely, complexity may be a hindrance to the work of air quality planning because it adds to computational burdens and makes the science more difficult to comprehend and communicate. Notably, very simple SOA schemes have performed as well or better than complex schemes in their ability to simulate ambient OA measurements when driven by ambient precursor measurements (Hodzic and Jimenez, 2011; Pai et al., 2020). Complex schemes can introduce responses to conditions, such as NO*x* concentration, that may be unexpected and should be overtly evaluated if they have policy relevance, such as the NO*x* effect on SOA yield from BVOC. Simple schemes with well-characterized SOA yields and responses can have an important place in air quality modelling to support decision making which includes studies that value the health-burdens of air pollution as well as

traditional emissions management planning.

In addition, a majority of the eight schemes reviewed here are based on the VBS approach and we expect that sampling a larger number of model schemes would not change this finding. VBS schemes have practical advantages because experimental studies frequently summarize their data (e.g., SOA yields, POA volatility) in a VBS frame which makes for direct translation of these data into a VBS model scheme. However, VBS data can be translated into a different frame (e.g., a two-product scheme) for SOA formation or for representing the partial evaporation of POA emissions, as illustrated by Huang et al. (2024). Therefore, scheme developers can consider using non VBS-based approaches to gain advantages of simplicity and efficiency. The findings summarized above underscore the importance of understanding the limitations of available SOA schemes when applied to air quality management and policy development. The choice of model/scheme can significantly influence the predicted SOA concentrations and their evolution over time, which in turn affects air quality forecasts, assessments and regulations.

DATA AVAILABILITY

The source data for the figures, including an example of the offline calculation (i.e. CMAQ AERO7), are available at Zenodo (https://doi.org/10.5281/zenodo.16757660). Calculation data for other species and schemes are available from the corresponding authors upon request.

AUTHOR CONTRIBUTIONS

G.Y. and L.H. designed the research. L.H. performed the data collection, yields calculation, and data analysis. ~~L.H.~~K.T. performed the box model calculation. L.H. K. T., and G.Y. wrote the manuscript. B. C., Z. W., K.T., P.V., and ~~P.V~~L.L. contributed to data analysis and revision of the manuscript. ~~Y.W. and L.L. contributed to the revision of the manuscript.~~ All authors contributed to the manuscript preparation and discussions.

ACKNOWLEDGMENTS

This work is supported by the Shanghai Technical Service Center of Science and Engineering Computing, Shanghai University. This study was financially supported by

the National Natural Science Foundation of China (Grant No. 42375103, 42375102) and Electric Power Research Institute (EPRI), Palo Alto, California.

COMPETING INTERESTS

The authors declare no competing interests.

REFERENCES

Appel, K. W., Bash, J. O., Fahey, K. M., Foley, K. M., Gilliam, R. C., Hogrefe, C., ... & Wong, D. C. (2021). The Community Multiscale Air Quality (CMAQ) model versions 5.3 and 5.3. 1: system updates and evaluation. *Geoscientific Model Development*, *14*(5), 2867-2897.

~~Ahmadov, R., McKeen, S. A., Robinson, A. L., Bahreini, R., Middlebrook, A. M., De Gouw, J. A., ... & Trainer, M. (2012). A volatility basis set model for summertime secondary organic aerosols over the eastern United States in 2006. *Journal of Geophysical Research: Atmospheres*, *117*(D6).~~

~~Beekmann, M., & Vautard, R. (2010). A modelling study of photochemical regimes over Europe: robustness and variability. *Atmospheric Chemistry and Physics*, *10*(20), 10067-10084.~~

Baboomian, V.J., Gu, Y. and Nizkorodov, S.A., 2020. Photodegradation of secondary organic aerosols by long-term exposure to solar actinic radiation. *ACS Earth and Space Chemistry*, *4*(7), pp.1078-1089.

Cappa, C. D., & Wilson, K. R. (2012). Multi-generation gas-phase oxidation, equilibrium partitioning, and the formation and evolution of secondary organic aerosol. Atmospheric Chemistry and Physics, 12(20), 9505-9528.

Chang, X., Zhao, B., Zheng, H., Wang, S., Cai, S., Guo, F., ... & Donahue, N. M. (2022). Full-volatility emission framework corrects missing and underestimated secondary organic aerosol sources. *One Earth*, 5(4), 403-412.

Chen, Q., Miao, R., Geng, G., Shrivastava, M., Dao, X., Xu, B., ... & Zhu, T. (2024). Widespread 2013-2020 decreases and reduction challenges of organic aerosol in China. *Nature Communications*, 15(1), 4465.

Crippa, M., Janssens-Maenhout, G., Dentener, F., Guizzardi, D., Sindelarova, K., Muntean, M., et al. (2016). Forty years of improvements in Eu ropean air quality: Regional policy-industry interactions with global impacts. *Atmospheric Chemistry and Physics*, 16(6), 3825–3841.

CHIMERE Users Guide (2023). https://www.lmd.polytechnique.fr/chimere/, accessed on Feb. 15th 2024.

Cholakian, A., Beekmann, M., Colette, A., Coll, I., Siour, G., Sciare, J.,... & Dulac, F. (2018). Simulation of fine organic aerosols in the western Mediterranean area during the ChArMEx 2013 summer campaign. *Atmospheric chemistry and physics*, *18*(10), 7287-7312.

Couvidat, F., Bessagnet, B., Garcia-Vivanco, M., Real, E., Menut, L., & Colette, A. (2018). Development of an inorganic and organic aerosol model (CHIMERE 2017 β v1. 0): Seasonal and spatial evaluation over Europe. *Geoscientific Model Development*, *11*(1), 165-194.

Donahue, N. M., Robinson, A. L., Stanier, C. O., & Pandis, S. N. (2006). Coupled partitioning, dilution, and chemical aging of semivolatile organics. *Environmental science & technology*, *40*(8), 2635-2643.

Donahue, N. M., Epstein, S. A., Pandis, S. N., & Robinson, A. L. (2011). A two-dimensional volatility basis set: 1. organic-aerosol mixing thermodynamics. *Atmospheric Chemistry and Physics*, *11*(7), 3303-3318.

Emery, C.A., Baker, K.R., Wilson, G.M. and Yarwood, G. (2024). Comprehensive Air Quality Model With Extensions, v7. 20: Formulation and Evaluation for Ozone and Particulate Matter Over the US. *Geoscientific Model Development Discussions*, *2024*, pp.1-48.

EPA. (2017). United States environmental protection agency: Overview of the clean air Act and air pollution. https://www.epa.gov/clean-air-act-overviewHonoré, C., Rouil, L., Vautard, R., Beekmann,, accessed on March 5th, 2026

M.,Bessagnet, B., Dufour, A., ... & Poisson, N. (2008). Predictability of European air quality: Assessment of 3 years of operational forecasts and analyses by the PREV'AIR system. *Journal of Geophysical Research: Atmospheres*, *113*(D4).

Hodzic, A. and Jimenez, J.L. (2011). Modeling anthropogenically controlled secondary organic aerosols in a megacity: A simplified framework for global and climate models. Geoscientific Model Development, 4(4), pp.901-917.

Hodzic, A., Jimenez, J. L., Madronich, S., Aiken, A. C., Bessagnet, B., Curci, G., ... & Ulbrich, I. M. (2009). Modeling organic aerosols during MILAGRO: application of the CHIMERE model and importance of biogenic secondary organic aerosols. *Atmos. Chem. Phys. Discuss*, *9*, 12207-12281.

Hodzic, A., Jimenez, J. L., Madronich, S., Canagaratna, M. R., DeCarlo, P. F., Kleinman, L., & Fast, J. (2010). Modeling organic aerosols in a megacity: potential contribution of semi-volatile and intermediate volatility primary organic compounds to secondary organic aerosol formation. *Atmospheric Chemistry and Physics*, *10*(12), 5491-5514.

Hodzic, A.; Kasibhatla, P. S.; Jo, D. S.; Cappa, C. D.; Jimenez, J. L.; Madronich, S.; Park, R. J. Rethinking the global secondary organic aerosol (SOA) budget: stronger production, faster removal, shorter lifetime. Atmos. Chem. Phys. 2016, 16, 7917−7941.

Huang, L., Liu, H., Yarwood, G., Wilson, G., Tao, J., Han, Z., ... & Li, L. (2023). Modeling of secondary organic aerosols (SOA) based on two commonly used air quality models in China: Consistent S/IVOCs contribution but large differences in SOA aging. *Science of The Total Environment*, *903*, 166162.

Huang, L., Zi'ang Wu, H. L., Yarwood, G., Huang, D., Wilson, G., Chen, H., ... & Li, L. (2024). An improved framework for efficiently modeling organic aerosol (OA) considering primary OA evaporation and secondary OA formation from VOCs, IVOCs, and SVOCs.

Huang, R. J., Zhang, Y., Bozzetti, C., Ho, K. F., Cao, J. J., Han, Y., ... & Prévôt, A. S. (2014). High secondary aerosol contribution to particulate pollution during haze events in China. Nature, 514(7521), 218-222.

Koo, B., Knipping, E., & Yarwood, G. (2014). 1.5-Dimensional volatility basis set approach for modeling organic aerosol in CAMx and CMAQ. *Atmospheric Environment*, *95*, 158-164.

Lane, T. E., Donahue, N. M., & Pandis, S. N. (2008). Simulating secondary organic aerosol formation using the volatility basis-set approach in a chemical transport model. *Atmospheric Environment,* 42(32), 7439-7451.

Li, J., Zhang, H., Li, L., Ye, F., Wang, H., Guo, S., ... & Hu, J. (2023). Modeling Secondary Organic Aerosols in China: State of the Art and Perspectives. *Current Pollution Reports*, 9(1), 22-45.

~~Luecken, D.J., Phillips, S., Sarwar, G. and Jang, C. (2008). Effects of using the CB05 vs. SAPRC99 vs. CB4 chemical mechanism on model predictions: Ozone and gas-phase photochemical precursor concentrations. *Atmospheric Environment*, *42*(23), pp.5805-5820.~~

~~Ma, S., Zhang, X., Gao, C., Tong, Q., Xiu, A., Zhao~~Li, H., ~~& Zhang, S. (2019). Simulating performance of CHIMERE on a late autumnal dust storm over Northern China. *Sustainability*, 11(4), 1074.~~

~~Ma, P.K., Zhao~~Zheng, B., Lei, Y., ~~Robinson, A.L., Worton, D.R., Goldstein, A.~~Hauglustaine, D., Chen, C., Lin, X., ... & He, K. (2024). Trends and drivers of ~~H., Ortega, A.M., Jimenez, J.L., Zotter, P., Prévôt, A.S., Szidat, S. and Hayes, P.L., 2017. Evaluating the impact of new observational constraints on PS/IVOC emissions, multi-generation oxidation, and chamber wall losses on SOA modeling for Los Angeles, CA. *Atmospheric chemistry and physics*, 17(15), pp.9237-9259.~~

Marais, E. A., Jacob, D. J., Jimenez, J. L., Campuzano-Jost, P., Day, D. A., Hu, W., ... & McNeill, V. F. (2016). Aqueous-phase mechanism for secondary organic aerosol formation from isoprene: application to the southeast United States and co-benefit of SO 2 emission controls. *Atmospheric Chemistry and Physics*, *16*(3), 1603-1618.

Murphy, B. N., Sonntag, D., Seltzer, K. M., Pye, H. O., Allen, C., Murray, E., ... & Robinson, A. L. (2023). Reactive organic carbon air emissions from mobile sources in the United States. *Atmospheric Chemistry and Physics*, *23*(20), 13469-13483.

Murphy, B. N., Woody, M. C., Jimenez, J. L., Carlton, A. M. G., Hayes, P. L., Liu, S., ... & Pye, H. O. (2017). Semivolatile POA and parameterized total combustion SOA in CMAQv5.2: impacts on source strength and partitioning. *Atmospheric chemistry and physics*, *17*(18), 11107-11133.

Murphy, B., W. Appel, J. Bash, K. Fahey, B. Henderson, Bill Hutzell, D. Kang, D. Luecken, R. Mathur, S. Napelenok, Chris Nolte, H. Pye, Jon Pleim, M. Qin, L. Ran, S. Roselle, G. Sarwar, D. Schwede, Q. Shu, AND T. Spero. Scientific and Structural Developments in CMAQv5.3. 2018 CMAS Conference, Chapel Hill, North Carolina, October 22 - 24, 2018.

Nault, B.A., Jo, D.S., McDonald, B.C., Campuzano-Jost, P., Day, D.A., Hu, W., Schroder, J.C., Allan, J., Blake, D.R., Canagaratna, M.R. and Coe, H. (2021). Secondary organic aerosols from anthropogenic volatile organic compounds contribute substantially to air pollution mortality. *Atmospheric Chemistry and Physics*NOx emissions in China since 2020. *Environmental Science and Ecotechnology*, 21(14), pp.11201-11224, 100425.

O'Brien, R.E. and Kroll, J.H. (2019). Photolytic aging of secondary organic aerosol: Evidence for a substantial photo-recalcitrant fraction. *The journal of physical chemistry letters*, *10*(14), pp.4003-4009.

Pankow, J.F. and Asher, W.E., 2008. SIMPOL. 1: a simple group contribution method for predicting vapor pressures and enthalpies of vaporization of multifunctional organic compounds. Atmospheric Chemistry and Physics, 8(10), pp.2773-2796.

Pai, S. J., Heald, C. L., Pierce, J. R., Farina, S. C., Marais, E. A., Jimenez, J. L., ... & Vu, K. (2020). An evaluation of global organic aerosol schemes using airborne observations. *Atmospheric Chemistry and Physics*, *20*(5), 2637-2665.

Murphy, B. N., & Pandis, S. N. (2009). Simulating the formation of semivolatile primary and secondary organic aerosol in a regional chemical transport model. *Environmental Science & Technology*, 43(13), 4722-4728.

Pankow, J. F. (1994). An absorption model of the gas/aerosol partitioning involved in the formation of secondary organic aerosol. *Atmospheric Environment*, *28*(2), 189-193.

Pennington, E. A., Seltzer, K. M., Murphy, B. N., Qin, M., Seinfeld, J. H., & Pye, H. O. (2021). Modeling secondary organic aerosol formation from volatile chemical products. *Atmospheric Chemistry and Physics*, 21(24), 18247-18261.

Pennington, Elyse A., Yuan Wang, Benjamin C. Schulze, Karl M. Seltzer, Jiani Yang, Bin Zhao, Zhe Jiang et al. "An updated modeling framework to simulate Los Angeles air quality–Part 1: Model development, evaluation, and source apportionment." *Atmospheric Chemistry and Physics* 24, no. 4 (2024): 2345-2363.

Pye, H. O. T., Chan, A. W. H., Barkley, M. P., & Seinfeld, J. H. (2010). Global modeling of organic aerosol: the importance of reactive nitrogen (NO*x* and NO_3). *Atmospheric Chemistry and Physics*, *10*(22), 11261-11276.

Pye, H.O., Pinder, R.W., Piletic, I.R., Xie, Y., Capps, S.L., Lin, Y.H., Surratt, J.D., Zhang, Z., Gold, A., Luecken, D.J. and Hutzell, W.T. (2013). Epoxide pathways improve model predictions of isoprene markers and reveal key role of acidity in aerosol formation. Environmental Science & Technology, 47(19), pp.11056-11064.

~~Pye, H.O., D'Ambro, E.L., Lee, B.H., Schobesberger, S., Takeuchi, M., Zhao, Y., Lopez-Hilfiker, F., Liu, J., Shilling, J.E., Xing, J. and Mathur, R. (2019). Anthropogenic enhancements to production of highly oxygenated molecules from autoxidation. *Proceedings of the National Academy of Sciences*, *116*(14), pp.6641-6646.~~

Pye, Havala OT, Cavin K. Ward-Caviness, Ben N. Murphy, K. Wyat Appel, and Karl M. Seltzer. "Secondary organic aerosol association with cardiorespiratory disease mortality in the United States." *Nature Communications* 12, no. 1 (2021): 7215.

Pye, H. O., Place, B. K., Murphy, B. N., Seltzer, K. M., D'Ambro, E. L., Allen, C., ... & Stockwell, W. R. (2023). Linking gas, particulate, and toxic endpoints to air emissions in the Community Regional Atmospheric Chemistry Multiphase Mechanism (CRACMM). *Atmospheric Chemistry and Physics*, *23*(9), 5043-5099.

Ramboll (2022). CAMx User's Guide, Version 7.20. Retrieved from https://www.camx.com/download/source/, accessed on Feb. 15th, 2024

Robinson, A. L., Donahue, N. M., Shrivastava, M. K., Weitkamp, E. A., Sage, A. M., Grieshop, A. P., ... & Pandis, S. N. (2007). Rethinking organic aerosols:

Semivolatile emissions and photochemical aging. *Science*, *315*(5816), 1259-1262.

~~Robinson, A.L., Donahue, N.M., Shrivastava, M.K., Weitkamp, E.A., Sage, A.M., Grieshop, A.P., Lane, T.E., Pierce, J.R. and Pandis, S.N., 2007. Rethinking organic aerosols: Semivolatile emissions and photochemical aging. *Science*, *315*(5816), pp.1259-1262.~~

Sarrafzadeh, M., Wildt, J., Pullinen, I., Springer, M., Kleist, E., Tillmann, R., Schmitt, S.H., Wu, C., Mentel, T.F., Zhao, D. and Hastie, D.R. (2016). Impact of NO x and OH on secondary organic aerosol formation from β-pinene photooxidation. *Atmospheric Chemistry and Physics*, *16*(17), pp.11237-11248.

Sasidharan, S., He, Y., Akherati, A., Li, Q., Li, W., Cocker, D., ... & Jathar, S. H. (2023). Secondary organic aerosol formation from volatile chemical product emissions: Model parameters and contributions to anthropogenic aerosol. *Environmental Science & Technology*, 57(32), 11891-11902.

~~Sciare, J., d'Argouges, O., Zhang, Q. J., Sarda-Estève, R., Gaimoz, C., Gros, V., ... & Sanchez, O. (2010). Comparison between simulated and observed chemical composition of fine aerosols in Paris (France) during springtime: contribution of regional versus continental emissions. *Atmospheric Chemistry and Physics*, *10*(24), 11987-12004.~~

Schell, B., Ackermann, I. J., Hass, H., Binkowski, F. S., & Ebel, A. (2001). Modeling the formation of secondary organic aerosol within a comprehensive air quality model system. *Journal of Geophysical Research: Atmospheres*, *106*(D22), 28275-28293.

Shrivastava, M., Easter, R. C., Liu, X., Zelenyuk, A., Singh, B., Zhang, K., ... & Tiitta, P. (2015). Global transformation and fate of SOA: Implications of low-volatility SOA and gas-phase fragmentation reactions. *Journal of Geophysical Research: Atmospheres*, *120*(9), 4169-4195.

Shrivastava, M., Fast, J., Easter, R., Gustafson Jr, W. I., Zaveri, R. A., Jimenez, J. L., ... & Hodzic, A. (2011). Modeling organic aerosols in a megacity: comparison of simple and complex representations of the volatility basis set approach. *Atmospheric Chemistry and Physics*, *11*(13), 6639-6662.

Strader, R., Lurmann, F., & Pandis, S. N. (1999). Evaluation of secondary organic aerosol formation in winter. *Atmospheric Environment*, *33*(29), 4849-4863.

Tsimpidi, A. P., Karydis, V. A., Pandis, S. N., & Lelieveld, J. (2016). Global combustion sources of organic aerosols: model comparison with 84 AMS factor-analysis data sets. *Atmospheric Chemistry and Physics*, 16(14), 8939-8962.

Vitali, Bruno, Manuel Bettineschi, Arineh Cholakian, Dino Zardi, Federico Bianchi, Victoria A. Sinclair, Johannes Mikkola et al. "Analysis of chemical and transport processes of biogenic aerosols over the northern Apennines: insights from the WRF-CHIMERE model." *Environmental Science: Atmospheres* 4, no. 9 (2024): 967-987.

Wildt, J., Mentel, T.F., Kiendler-Scharr, A., Hoffmann, T., Andres, S., Ehn, M., Kleist, E., Müsgen, P., Rohrer, F., Rudich, Y. and Springer, M. (2014). Suppression of new particle formation from monoterpene oxidation by NO*x*. *Atmospheric Chemistry and Physics*, *14*(6), pp.2789-2804.

WRF-Chem version 4.4 Users Guide. (2022). https://ruc.noaa.gov/wrf/wrf-chem/Users_guide.pdf, accessed on Feb. 15th 2024.

~~Xu, L., Guo, H., Boyd, C. M., Klein, M., Bougiatioti, A., Cerully, K. M., ... & Ng, N. L. (2015). Effects of anthropogenic emissions on aerosol formation from isoprene and monoterpenes in the southeastern United States. *Proceedings of the National Academy of Sciences*, 112(1), 37-42.~~

Yarwood, G. and Tuite, K., 2024. Representing Ozone Formation from Volatile Chemical Products (VCP) in Carbon Bond (CB) Chemical Mechanisms. Atmosphere, 15(2), p.178.

Yu, H., Møller, K.H., Buenconsejo, R.S., Crounse, J.D., Kjaergaard, H.G. and Wennberg, P.O., 2023. Atmospheric Photo-Oxidation of 2-Ethoxyethanol: Autoxidation Chemistry of Glycol Ethers. The Journal of Physical Chemistry A, 127(45), pp.9564-9579.

Zawadowicz, M. A., Lee, B. H., Shrivastava, M., Zelenyuk, A., Zaveri, R. A., Flynn, C., ... & Shilling, J. E. (2020). Photolysis controls atmospheric budgets of biogenic secondary organic aerosol. Environmental Science & Technology, 54(7), 3861-3870.

Zhang, Q~~., Laurent, B., Velay-Lasry, F., Ngo, R., Derognat, C., Marticorena, B., & Albergel, A. (2012). An air quality forecasting system in Beijing-Application to the study of dust storm events in China in May 2008. *Journal of Environmental Sciences*, *24*(1), 102-111.~~

~~Zhang, Q~~. J., Beekmann, M., Drewnick, F., Freutel, F., Schneider, J., Crippa, M., ... & Perrussel, O. (2013). Formation of organic aerosol in the Paris region during the MEGAPOLI summer campaign: evaluation of the volatility-basis-set approach within the CHIMERE model. *Atmospheric Chemistry and Physics*, *13*(11), 5767-5790.

Zhang, X., Cappa, C. D., Jathar, S. H., McVay, R. C., Ensberg, J. J., Kleeman, M. J., & Seinfeld, J. H. (2014). Influence of vapor wall loss in laboratory chambers on

yields of secondary organic aerosol. *Proceedings of the National Academy of Sciences*, 111(16), 5802-5807.

Zhao, D., Schmitt, S. H., Wang, M., Acir, I. H., Tillmann, R., Tan, Z., ... & Mentel, T. F. (2018). Effects of NOx and SO2 on the secondary organic aerosol formation from photooxidation of α-pinene and limonene. Atmospheric Chemistry and Physics, 18(3), 1611-1628.

Zhao, Y., Hennigan, C. J., May, A. A., Tkacik, D. S., de Gouw, J. A., Gilman, J. B., ... & Robinson, A. L. (2014). Intermediate-volatility organic compounds: a large source of secondary organic aerosol. *Environmental Science & Technology*, *48*(23), 13743-13750.

Zhao, B., Wang, S., Donahue, N. M., Jathar, S. H., Huang, X., Wu, W., ... & Robinson, A. L. (2016). Quantifying the effect of organic aerosol aging and intermediate-volatility emissions on regional-scale aerosol pollution in China. *Scientific reports*, 6(1), 28815.